Theses and Dissertations

2010

Development of a protocol for 3-D reconstruction of brain aneurysms from volumetric image data

David Michael Welch
University of Iowa

Recommended Citation

Welch, David Michael. "Development of a protocol for 3-D reconstruction of brain aneurysms from volumetric image data." MS (Master of Science) thesis, University of Iowa, 2010.
http://ir.uiowa.edu/etd/1189.

DEVELOPMENT OF A PROTOCOL FOR 3-D RECONSTRUCTION OF
BRAIN ANEURYSMS FROM VOLUMETRIC IMAGE DATA

by

David Michael Welch

A thesis submitted in partial fulfillment of the
requirements for the Master of Science
degree in Biomedical Engineering in the
Graduate College of The
University of Iowa

July 2011

Thesis Supervisor: Professor Madhavan L. Raghavan

Graduate College
The University of Iowa
Iowa City, Iowa

CERTIFICATE OF APPROVAL

_____

MASTER'S THESIS

_____

This is to certify that the Master's thesis of

David Michael Welch

has been approved by the Examining Committee
for the thesis requirement for the Master of
Science degree in Biomedical Engineering at the July 2011
graduation.

Thesis Committee: _____
                   Madhavan Raghavan, Thesis Supervisor

                  _____
                   Sarah Vigmostad

                  _____
                   David Hasan

                  _____
                   Thomas Brown

To my wife, Michelle and my son Jonathan:
Our family is forever

ACKNOWLEDGMENTS

TABLE OF CONTENTS

LIST OF TABLES

Table

LIST OF FIGURES

Figure

CHAPTER 1
INTRODUCTION

1 .1   Motivation

In the last half-century, there has been an explosion of medical imaging applications and practices. As computing power has increased, segmentation, reconstruction, and modeling schemes have become more sophisticated, complex, and technically challenging. Unfortunately, these developments have also contributed to a decrease in the ability within the scientific community to accomplish reproducible research in these areas. "In-house" code, potentially marketable advances, and unique data sets have traditionally kept peers from policing themselves and independently verifying results [38]. Historically, segmentation methods have focused on the performance of the method and overlooked reproducibility. Vannier and Haller in 1998 stated that the "(e)valuation of biomedical image segmentation is based on the efficiency of specific methods in terms of the time (computational effort) required to achieve a solution, storage space, real time capability, and statistical measures of classifier performance including accuracy (multiclass), measures of agreement (kappa, group correlation), and precision (repeatability)." As image segmentation becomes more common in clinical and research investigations, it becomes increasingly difficult to compare methods for precision. Schwab, Karrenbach, and Claerbout suggest that papers are becoming "merely the advertisement of scholarship" [51]. Since the end goal of our results are clinical application, the validity and stability of these methods are an important topic of interest to the medical imaging community at large.

Due to the rarity of the condition among the general populace and the time constraints for gold-standard manual segmentation, studies that segment and model patient-specific aneurysms have traditionally used a small number of patients (< 32) and often only a few expert users [6, 7, 17, 18, 22, 33, 40, 44, 46, 47]. Furthermore, it is advantageous for large-scale investigations to report rapid application development [9]. Studies that include larger populations often do not examine the segmentation trends between users [7] and those that do compare segmenters fail to report a codified protocol or training method for those users [23]. It is important that these applications be robust under different operator bias such as experience level and psychophysiological perception [3,5]. The ability to validate modeling methods over large clinical data sets demands that the segmentation methods be codified and address a large variation of image quality, user understanding, and segmentation methods.

1 .2   Background

Cerebral aneurysms (CA) are permanent dilations of the arterial vasculature in the head and neck. These arterial malformations differ from abdominal aortic aneurysms (AAA) in scale and geometry. While both develop radially, CA expansion tends to be localized on a preferred side, whereas AAAs are more likely to distend uniformly. Cerebral aneurysms have the potential to rupture, causing spontaneous subarachnoid hemorrhage [37, 59]. Furthermore, unruptured cranial aneurysms can cause increased pressure to surrounding tissues creating headaches and/or cranial neuropathies [29, 59]. Aneurysm prevalence among the general populace is close to 2% [12, 26, 27] and that 10% − 20% of ruptured aneurysms result in death [59].

To treat CA, endovascular coiling and surgical clipping are the current interventional methods available. Coiling has been shown to have decreased risk and equivalent effectiveness compared to surgical intervention [57]. Due to the aneurysm location within the brain or risk involved with treatment, one or both of these methods may be unavailable to the clinician. Therefore, providing a reliable way to quantify the risk of a "wait and see" approach is important in patient treatment decisions.

Traditionally, clinical wisdom has held that large CAs ($> 10mm$) were at risk of rupture, but studies have shown that small aneurysms may present just as great a risk [11, 19, 48, 49]. Small aneurysm segmentation is needed to allow for biomechanical studies to study the rupture mechanisms present in these cases. These small pathological structures present new challenges to vessel segmentation, such as an emphasis on segmentation algorithms with sub-voxel precision and lower signal-to-noise ratios (SNR) in image acquisition.

The Vascular Modeling Toolkit (VMTK) is a Python-based library of scripts designed to segment tubular and spherical structures with subvoxel precision [1]. VMTK collects many algorithms from the open source Image Processing Toolkit (ITK) [25] and the Visualization Toolkit (VTK) [50] and scripts them into cohesive functions that can be pipelined into more elaborate processes. The ITK components are geared specifically towards segmentation of cylindrical geometries and analysis, while VTK is used predominantly to handle data rendering and visualization (Sec. 1 .2.3). Thus, VMTK also allows researchers to make rapid investigations, which increases the likelihood that studies using this toolkit will be investigated further, an advantage over costlier, specialized commercial applications.

In development and validation of VMTK, Antiga *et al.* [2] encouraged studies that examine the robustness and precision of their toolkit. They state that "(v)alidation studies on physical or virtual phantoms. . . , and patient studies based on repeated and multi-modality scans. . . , have to be encouraged for specific flow domains and quantities of interest." Unfortunately, the ability to pipeline functions and to interact with data means that user understanding of methods, scripts, and options makes study validation between investigators difficult due to increased customization. For instance, pipeline development for a specific task can vary between investigations and between investigators. Secondly, users choose the type of inital segmentation methods (threshold, isosurface, colliding fronts (A.1), fast marching (A.2), threshold limits, and initial seed points. Finally, the results are also dependent on the local image composition, anatomy, and modality. Studies need to be conducted that examine the user's influence on the final segmentations.

To decrease the variability in segmentation results, our protocol makes use of many of the advanced pipelines developed for VMTK so that a user is only needed to interact at branch points of the pipeline, to create the initial segmentations of the vasculature, and to input smoothing parameters of the boundary evolution. It also provides guidelines for modalities, as well as guidelines for segmentation, and criteria for choosing seed points and evolution parameters.

1 .2.1 Previous Work

1 .2.1.1 Mechanics and Shape

Aneurysm rupture is a mechanical failure of the vascular tissue, so it is natural that rupture prediction should be concerned with the mechanical properties

of aneurysms. For instance, de la Monte [12] studied the risk factors for development of berry (saccular) aneurysms in 170 cadaveric patients and concluded that the pathogenesis of aneurysm rupture is likely due to mechanical predisposition. Foutrakis *et al.* [20] found that saccular aneurysms tended to form on the flow impinging wall in curved and bifurcated cerebral arteries, postulating that fluid forces initiated aneurysm formation and rupture. Singh *et al.* [54] created theoretical 'pre-anerysmal' vessels from two patient scans and simulated normal and increased blood viscosity (due to smoking or hypertension) to study wall sheer stress (WSS) at the locations where aneurysms had formed. They found that WSS was high at those locations with both viscosities, but the increased viscosity simulation was the highest of the two.

Kyriacou and Humphrey [30] proposed that shape, loading, and material properties were essential to rupture risk through analysis of multiaxial stress and strain computation. A study of two dissected anerysms by Seshaiyer *et al.* tried to capture the multiaxial material properties of aneurysms and demonstrated the difficulty in obtaining valid specimens as well as measuring material properties in three dimensions [52]. Computer modeling of aneurysms is an attractive alternative method for large studies, but it requires accurate material properties, fluid characteristics, and geometry.

Even without mechanical analysis, aneurysm shape has been understood to be a noteworthy predictor of rupture risk. Ujiie *et al.* studied the incidence of aneurysm rupture for a retrospective population of patients ($n = 44$) and they classified shape in gross terms (round, oval, bar), though they didn't investigate their influence on rupture [55]. In another paper, they investigated how shape influenced the CFD of aneurysms in rabbit models and found that slow flow near the aneurysm dome was

charateristic of aspect ratios (see Section 2.3) > 1.6 and provided an environment where pathologic material remodeling could occur [56].

Banatwala *et al.* [6] observed that the historical emphasis on the aneurysm maximum diameter as a predictor for rupture comes from a misinterpretation of the law of Laplace and propose that geometry, material properties and applied loads should determine the risk of aneurysm rupture. This agreed with the findings of Elger [16] studying abdominal aortic aneurysms (AAA), who showed that maximum curvature, not diameter affected hoop stresses more and was a better predictor for rupture risk.

1.2.1.2 Shape Characterization

Shape charateristics of aneurysms can affect the treatment planning by clinicians. In 1999, Parlea *et al.* devised a set of geometric ratios to assist in treatment planning [43]. In a study of 62 patients, Johnston *et al.* investigated how shape characteristics affected clinical planning and found high aspect ratio was the largest excluding factor for coiling [29]. These studies provided clinical treatment information, but had the disadvantage of providing no insight on mechanical loading within aneurysms or rupture risk assessment.

Since then, work has been conducted to ascertain how shape index measures can provide the clinician and patient with risk information. Raghavan [46] and Ma [33] studied several shape indices studies in order to develop metrics that could be used for treatment decision, presurgical planning, and biomechanical analysis. They developed 2- and 3-D shape indices (see Table 2.3 for a partial list). The shape indices developed by Ma and Raghavan have been studied by both Dhar [14] and Rahman [47]. They proposed a new index, size ratio, defined as the ratio of

the maximum diameter of the aneurysm to the diameter of the parent vessel. Hoh studied rupture risk using the 1- and 2-D indices in Raghavan and found that aspect ratio and bottleneck factor correlated with rupture risk [24] in their study.

In addition, Banatwala et al. [6] charaterized shape using Legendre polynomials and Millan et al. [39, 40] have applied 3D moment invariants to classify shape.

Lastly, de Rooij suggests that the location of aneurysms is an influencing factor for rupture risk that should be addressed simultaneously with aneurysm shape charaterization [13].

1 .2.1.3 Segmentation Validation

Segmentation accuracy of the vessel wall is difficult in imaging data that only captures the lumen volume, therefore precision is used as a surrogate. This is a time-consuming process for manual, 'gold-standard' segmentation and most early studies using manual tracings avoided examining operator bias. As techniques became faster and more automated, the need for precision studies became more necessary. Cebral noted that for CFD models "(s)pecification of the correct physiologic flow conditions for each individual patient is important" [8], which includes patient geometry as well as fluid and material properties.

Antiga et al. [2] perfomed a validation study of VMTK using a rigid, patient-specific phantom created from a carotid bifurcation segmentation made using the VMTK method. They scanned the phantom using CTA and MRA (gadolinium-enhanced, axial & coronal) with clinical settings, segmented the resulting DICOM image sets using two different finite difference approximations, and compared the registered segmentations against the original, ground-truth segmentation. They found good agreement between models for both approximation schemes and the

highest accuracy with CTA. Unfortunately, the simplicity of the segmented geometry and the absence of image artifacts in the phantom data sets (i.e. bone, chaotic flow, etc.) means that more investigation is needed to reliably assess VMTK's reproducibility on large patient data sets (see Piotin, 2003 [45]).

Hernandez *et al.* [23] performed a patient study that compared the neck, width, and depth measurements from 40 automated segmentations against two neuroradiologists using MIPs. They found no significant difference between measurements done automatically or manually and that small changes in viewpoint could result in manual measurement error. The importance of comparing the automated method results against clinical observation highlights an important point in regards to segmentation algorithms: clinicians are loath to trust novel, automated methods in their decision planning without thourough testing and validation of the methods.

1.2.2 Imaging Modalities

Imaging techniques of intracranial aneurysms have different advantages and trade-offs. Digital subtraction angiography (DSA) is the gold-standard for aneurysm imaging, but has a morbidity rate of $1-2\%$. Computed tomographic angiography (CTA) uses less contrast and is a safer alternative, but still requires ionizing radiation. Magnetic resonance (MR) angiography can use magnetic flow effects (time-of-flight, phase-contrast) or magnetically susceptible dye (gadolinium-enhanced), which may be more tolerable for patients with co-morbidity concerns [58].

1.2.2.1 Computed Tomography Angiography

CTA is used clinically to diagnose cerebral aneurysms in patients. A radio-opaque dye (water-soluble iodine) is introduced into the venous system by means of

an intravenous line in the arm or hand. A small amount of dye is injected and timed to determine the appropriate scanning time for the the region of interest (ROI). The resulting scan features the intensity values of voxels containing arteries that are signifcantly higher than the surrounding tissue. In this manner, a 3D reconstruction of the patient artery geometry can be developed using the appropriate segmentation techniques and a priori knowledge of human anatomy. Due to the hightened signal amplitude of lumen in CTA, intensity-based segmentations near bone are difficult due to comparable signal strengths [8]. CTA has been found to have good agreement with DSA [60].

1.2.2.2 Magnetic Resonance Angiography

Magnetic resonance (MR) angiography consists of two major techniques: contrast-enhanced and time-of-flight (ToF) imaging. Contrasted MR (MRA) works much the same as CTA in that a dye is administered that produces a higher signal (in this case, radio frequency or RF) than the surrounding tissue. The contrast for MR is a gadolinium-based dye. White found that CTA performs marginally better than MR, though not signifcantly [61].

Time-of-flight (ToF) MR is a method that takes advantage of the spacial displacement of blood within the vessels. In a given plane, the magnetic field aligns the proton spins uniformly, which are then excited to saturation with rapid RF pulses. Blood flowing into this plane from elsewhere is excited and emits a stronger signal than the saturated static tissue. If this material remains within the plane, it will become saturated, therefore ToF is susceptible to signal loss in areas of turbulent flow. Therefore, MRToF tends to underestimate the lumen of large aneurysms [4,21] and may exaggerate stenosis [15, 41].

A phantom study by Isoda [28] concludes that MRA performs better than MRToF for aneurysm lumen imaging, provided the scan is taken as the contrast fills the aneurysm. Despite these caveats, several investigations [31, 60] concluded that MRToF was comparable to DSA in sensitivity, accuracy, and correlation, though Okahara *et al.* noted careful attention and skill is required around the internal carotid artery (ICA) and the anterior cerebral artery (ACA) [42].

1.2.2.3 Imaging Limitations

In all the methods mentioned, only the vessel lumen can be imaged with any accuracy. Therefore, the aneurysm inner wall geometry is achieved by assuming that there is no intraluminal thrombus in the aneurysm sac.

1.2.3 Toolkits

1.2.3.1 ITK

ITK is a toolkit developed under a contract awarded by the US National Library of Medicine in 1999 to six consortium members: GE Corporation R&D, Kitware, Inc., MathSoft (Insightful), University of North Carolina, University of Tennessee, and University of Pennsylvania. It was written in C++ so as to be generic and highly-efficient at processing large amounts of data. A few of its goals are to create a repository of fundamental image processing algorithms and grow a community of software users and developers [25].

1.2.3.2 VTK

VTK was orginally written as part of a textbook on 3D graphics and visualization. At its core, VTK does 3D graphics, modeling, image processing, and volume

rendering. Written in C++, it supports parallel processing to further increase the speed of interaction with users [50].

1 .2.3.3 VMTK

ITK and VTK were developed to facilitate peer collaboration and review [50, 62]. These projects attempt to collect algorithms, methods, and tools in a consistent way such that investigators can use the same code to compare and develop methods of segmentation and visualization. The level of complexity within these toolkits has grown over their existence and child applications and scripting libraries have resulted from them. One of these scripting libraries is VMTK [1], which collects many algorithms in ITK and VTK that are geared specifically towards analysis and segmentation of cylindrical geometries. VMTK is written in Python, a scripting language noted for its ability to quickly build working code. VMTK is designed to allow researchers to make rapid investigations by handling the visualization environment through VTK-based scripts and the image processing through ITK- and VTK-based scripts.

Algorithms that rely on user-selected points have the potential for largely different results if they are sensitive to the initial input conditions. For many medical image processing applications, user-defined initial starting points are often necessary, either due to clinical acceptance or the difficulty of automated feature recognition. VMTK makes use of user-defined starting points for two methods of image segmentation: colliding fronts (A.1) and fast marching (A.2).

VMTK segmentation uses level set and fast marching methods developed by Sethian and others [53] and is used in a wide varitey of applications, both in medical image analysis and others [10, 34, 35, 63]. Segmentation is initially made by

a single segmenter and then evolved by a speed function constrained by user input and image intensities. Both methods attempt to evolve a moving interface, either from an initial value or a boundary value formation (A.3) which results in surfaces with sub-voxel accuracy.

1 .3   Objectives

Our protocol is designed to allow inexperienced users with minimal training produce segementations comparable to experienced ($<$ 6 months) users. Our protocol should also be easy to use and control the segmentation workflow for the majority of challenges encountered with cerebral anerysms. Segementations produced from novice users will have shape indices statistically similar to experienced, expert users.

CHAPTER 2
MATERIALS AND METHODS

2 .1   Overview

In an effort to create reproducible research in vessel segmentation and analysis, our cerebral aneurysm reconstruction protocol is developed for a large data set ($>$ 32) comprised of the three most popular 3D vessel imaging techniques (CTA, MRA, MRToF) with varying image resolutions and scanners to minimize user influence from image to surface mesh. This protocol allows investigators to report a small number of options (evolution parameters) in order to facilitate peer-review and comparisons of results on separate data sets when data cannot be shared due to legal/ethical restrictions.

Our protocol employs the algorithms developed within VMTK. This toolkit is open source and thereby encourages validation of our results by latter studies. The goal of our protocol is to minimize segmentation variation between users for a given patient scan. Early on it was decided that image filtering would not implemented in any of our images since making a single filter standard would not be appropriate for all images, studies, and modalities.

Therefore correctly identifying and segmenting the aneurysms relies only on the image quality, resolution, and user skill. In order to develop a protocol that is appropriate for a large data set, a database with sufficiently large image characteristics and challenges needs to be obtained. Our database consists of clinical patient scans from three institutions (Massachusetts General, Thomas Jefferson University, and Pennsylvania State University Hospital at Hershey) ($n = 71$).

2 .2   Segmentation Protocol

The protocol is designed to be a GUI-based workflow application, removing much of the technical and scripting aspects of vessel segmentation currently in VMTK and standardizing segmentation methods among researchers. GUI handling is done by Zenity (http://live.gnome.org/Zenity), a GTK-based tool designed to be run from the command line and shell scripts. GTK is a toolkit designed for cross-platform compatibility and easily implemented application programming interfaces (API). Currently, the protocol utilizes Zenity's file selection, list, message, and text entry windows.

For image visualization and segmentation, our protocol has hard-coded VMTK script pipelines and file nomenclature, allowing users to consistently explore large databases without any loss of data organization or variations in methods from user to user.

2 .2.1   Workflow

The user is prompted to select a destination folder for all output files. This folder should be unique to that user, as any subsequent runs of the protocol into that destination folder will overwrite the files created previously.

The user is then asked to input a patient identfication number. Currently the range of valid patient IDs is

$$fl(x/1000) * 1000 < x < (fl(x/1000) + 1) * 1000$$

where $x = 1, 2, 3, 4$. This ID number becomes the first component of the resulting filename strings (i.e. Subject 1073 will produce filenames beginning with "1073"). Once an appropriate ID number is given, the user needs to direct the protocol to the correct DICOM scan. To do this, the protocol employs MIPAV, a DICOM medical

image viewer developed by the NIH Center for Information Technology [36].

The user can interactively explore the data folder tree[1], view the images, read header information, and identify the appropriate scan to reconstruct based on the the study criteria (resolution, modality, vessel contrast, presence of artifacts, etc.). The user guides a file navigation GUI to the DICOM folder containing the appropriate scan. In this environment, the user identifies the aneurysms from the locations given clinically[2]. The user inputs the location of the aneurysm from a list of 15 common locations (including hemisphere location) or manually enters the location, if it is not included in the list.

The protocol creates a maximum intensity projection (MIP) of the complete data set at this point[3]. Using VMTK, the protocol loads the data set in an interactive window where the user can manipulate three image planes (transverse, sagittal, coronal). Typing "i" in the window, the user creates a volume of interest (VOI) containing the aneurysm and contiguous vessels using an interactive box to select the bounds of the VOI. This file is saved as "patientID_location.vti", where patientID is the four digit patient ID number and location is the user identified location. A MIP of this file is also created[4].

---

[1]Since VMTK reads in an entire DICOM folder, the source data may need to be separated before the protocol can process it. For our study, data was sorted at the time of database uploading using in-house code.

[2]Larger aneurysms (¿10 mm) should be recognizable to a user familiar with the anatomy in question and clinical knowledge may be blinded from the user for increased rigor.

[3]Initially, MIPs were to be used to identify aneurysms in 3D space without clinician input. Unfortunately, VMTK does not currently allow interactive MIP brightness/contrast manipulation, and 3D interaction (rotation) with MIP files is not fast enough for real-time identification of aneurysms. We anticipate this deficiency to be addressed in future versions.

[4]File nomenclature is important since the protocol uses filenames to recognize data files with similar extensions.

2 .2.1.1 Sigmoids

Assuming the user wishes to segment the VOI during this session, the protocol queries the user about the air and bone content of the image. If there is air or bone near the vasculature, the steep gradient change can interfere with the segmentation. When a steep gradient is present in discrete data, the interpolated values between are roughly linear, even though the underlying anatomy has discontinuities. VMTK handles this by creating 'no-go' zones, called sigmoids. These sigmoids are surface boundaries that prevent the level set evolution from including any volume bounded by them. If appropriate, the user can create up to two sigmoids for a VOI: bone and air. This procedure is most helpful for CTA scans of carotid aneurysms, since they are often in close proximity to both bone and air volumes.

Sigmoids are created using a simple thresholding for the initial segmentation. Once created, the user can examine it within the VOI and verify that it is correct. If not, the user can choose a different values until they find a suitable choice. Once made, the surface is smoothed using default level set smoothing parameters[5].

2 .2.1.2 Segmentations

Now the user is asked to segment the contiguous vessels about the aneurysm, if no previous segmentation file is present. Vessel segmentation is accomplished with the colliding fronts algorithm (A.1). The user identifies two voxels, a start point and an end point within the lumen of a vessel to be segmented. The resulting initial segmentation is displayed and the user can examine it interactively. If it is unacceptable (e.g. it includes non-vessel volume), the user can repeat the process until satisfied. Once the segmentation is made, the user can add additional volumes

---

[5]300 iterations, 0 propagation weighing, 0 curvature weighing, 1 advection weighing

by repeating the process. Once all vessels are created, this initial segmentation file is saved. It can be added to, if needed, by running the protocol again from the beginning. After the initial segmentation is complete, creating a surface with sub-voxel precision is done with level sets smoothing. The user inputs the number of iterations and three weighing parameters controlling the propagation, curvature, and advection of the evolved surface (A.3), inspects the results, and accepts the output or repeats the level sets process.

The aneurysm segmentation is computed with the fast marching algorithm (A.2). This method accepts numerous start and end points. Our protocol constrains the method to a single start point located at the center of the aneurysm. The end points are chosen as the maximum distance from the center in the cardinal directions, plus one end point in the center of the parent vessel. This last point ensures the volume that will merge with the previous vessel segmentation. Again, the user smooths the geometry using the level set evolution with seperate inputs for the aneurysm geometry (Fig.2.1).

Once the algorithm is complete, VMTK displays the evolved surface for review and verification by the user. The evolution can be recomputed with different parameters and displayed until the user is satisfied. We found the time between evolution to be on the order of 5–7 minutes, allowing users to compare a evolved surface with previous choices.

The final evolved surface is saved and the process of segmentation is repeated for the aneurysm geometry, with the exception that the initial segmentation uses a fast marching segmentation algorithm (A.2), that is more appropriate for spherical structures.
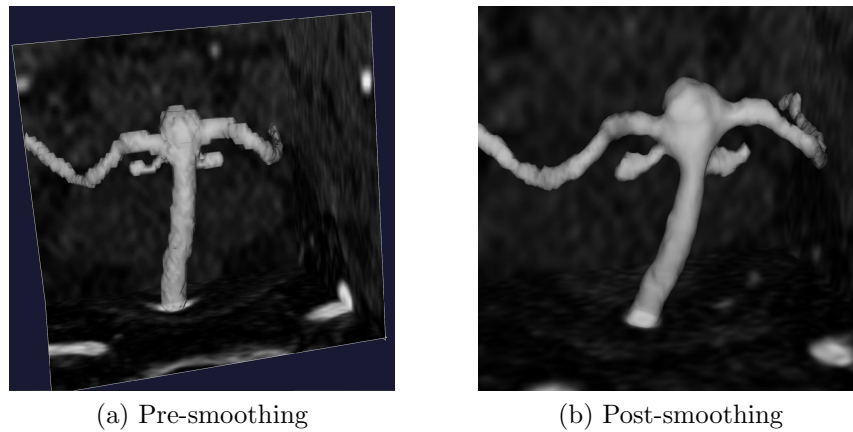
(a) Pre-smoothing (b) Post-smoothing

Figure 2.1: left) Segmented vessels and aneurysm before smoothing computed, right) Smoothed segementation using 300 iterations without any weighing of curvature or propagation.

2 .2.1.3 Mesh Creation

Once the two segmentations (vessels and aneurysm) are created, they are combined as a union of the two surfaces. This combined segmentation is then passed to the marching cubes algorithm (A.4) for mesh creation. The user then reviews the mesh to verify that the geometry of the segmentation is preserved. There are cases when aneurysm and vessel surfaces are near each other at locations away from the aneurysm neck and elements of the mesh can incorrectly bridge the small gap between the structures. If this is so, the user can choose to incorporate a shrinking term α to the surfaces, thereby increasing the distance between segmentation boundaries. The term α is a constant, $0 < \alpha < 1$, and is applied to aneurysm and vessel segmentations separately.

Once the mesh is verified, it is then written to a Tecplot[6] file and the program

---

[6]Tecplot, Inc., Bellevue, WA

is complete.

2 .2.2   Development and Testing

To develop and test the protocol, we created three data sets: development, training, and testing. The development set was made to help codify and refine the protocol, in concert with consultation from experienced segmenters. The testing set was created to test the protocol's agreement between experienced (expert) and inexperienced (novice) users. The training set's purpose is to train the novice users on the protocol and segmentation.

2 .2.2.1   Patient Population

Our database is composed of 136 patients identified with 158 aneurysms collected from three institutions: Massachusetts General Hospital (MGH), Pennsylvania State University(PSU), and Thomas Jefferson University (TJU). Clinical shape classifications (saccular, fusiform, other) exists for 131 of the aneurysms identified. Of the 136 patients, ten were selected for inclusion in our development set and ten were selected for the testing set. Due to the unique challenges CTA offered, we wished to have CTA over-represented of the three modalities in our development and testing sets. Therefore the development set was composed of four patients from our CTA data, three from MRA and MRToF, while the testing set consisted of six CTA, and two MRA and MRToF. The selection process divided our database by modalities and then randomly selected from those subgroups.

Also, internal carotid artery (ICA) aneurysms constitute almost half of our current database. This location presents the greatest challenge for segmentation in CTA data (2 .2.1.1).

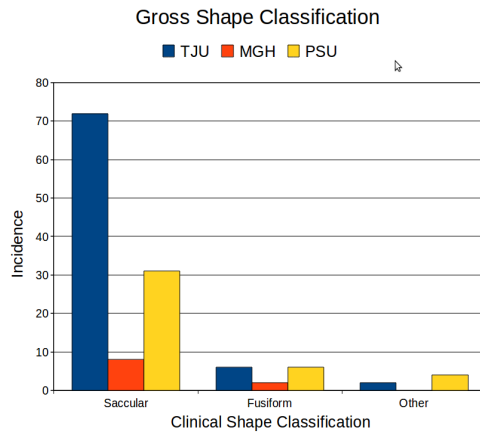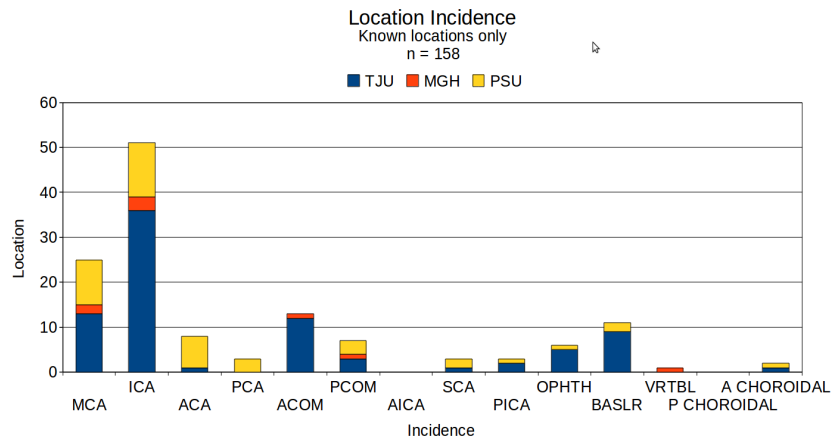Figure 2.2: Clinical shape classifications as identified by the submitting clinician (n=131).

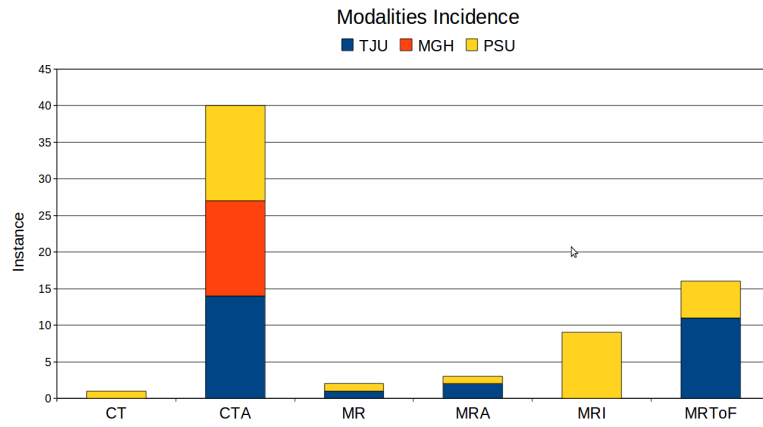Figure 2.3: The aneurysm location distribution of our database (n=158).

Figure 2.4: Modality distribution of database. CT, MR, and MRI may indicate scans without contrast or scans not reliably identified by their source institution.
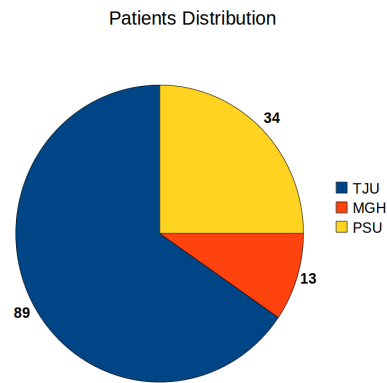
Figure 2.5: Number of patients provided from participating institutions.
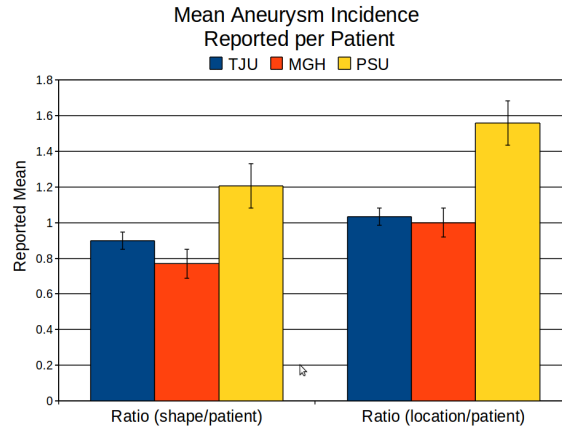
Figure 2.6: Patient mean aneurysm occurance in our study. Error bars indicate the standard statistical error.

Of the four unused cases, one patient was only successfully segmented by three of the four users (one expert, two novices). Another MRToF presented a flow artifact within the parent vessel (Fig. 2.7) of the aneurysm and prevented segmentation of the aneurysm/vessel interface.

Two aneurysm geometries were poorly suited for our method of aneurysm separation. One aneurysm was located in the C5 segment of the ICA, extending internally in the plane of the carotid bend (Fig. 2.8). The neck of the aneurysm originates from the interior side of the bend, an area of high curvature. The aneurysm shape was roughly spherical, filling much of the space between the C6 and C4 segments, Seperating the aneurysm using a plane was not possible without losing a significant portion of the aneurysm. The other aneurysm was a branch point aneurysm, with no definable aneurysm neck.

The training set was composed of three scans of an anatomical silicone flow model, one scan from each of our three modalities. A silicone dynamic flow model[7]

[7]ELASTRAT H+N-R-A-002, Shelley Medical Imaging Technologies
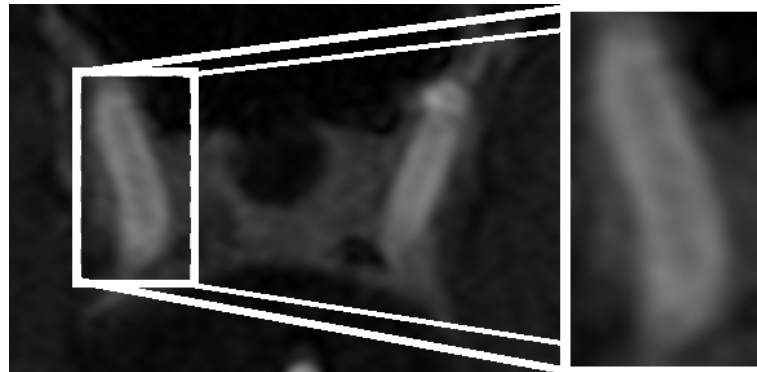
(a) Transverse view of C4 section of ICA
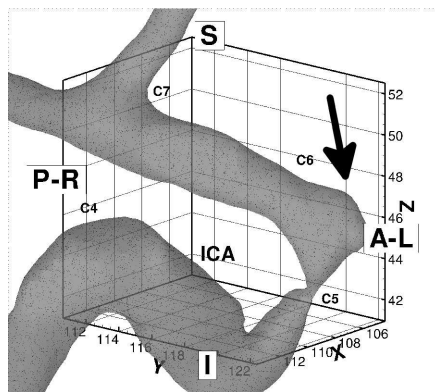
(b) Expert 1
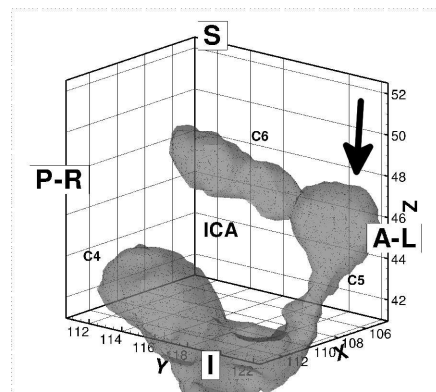
(c) Expert 2
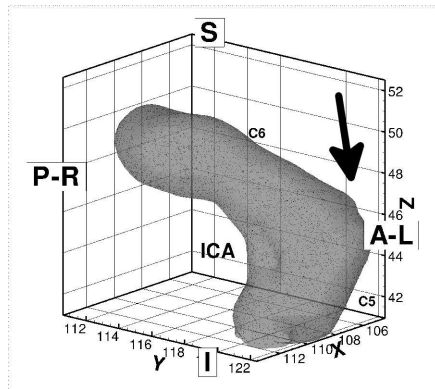
(d) Novice 1
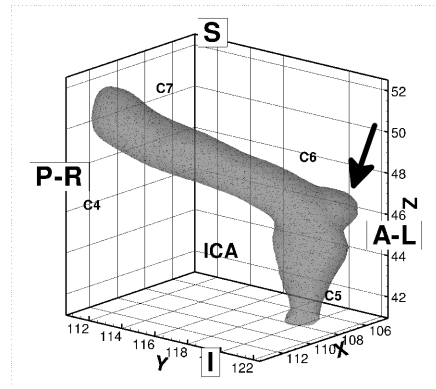
(e) Novice 2

Figure 2.7: Intensity variation within a vessel can severely affect the outcome of the segmentation if surrounding tissue has a overlapping intensity profile. Sigmoid isosurfaces cannot be choosen to correctly bound the levelset evolution, forcing segmenters to produce unacceptable vessel segmentations.

(a) Expert 1

(b) Expert 2

(c) Novice 1

(d) Novice 2
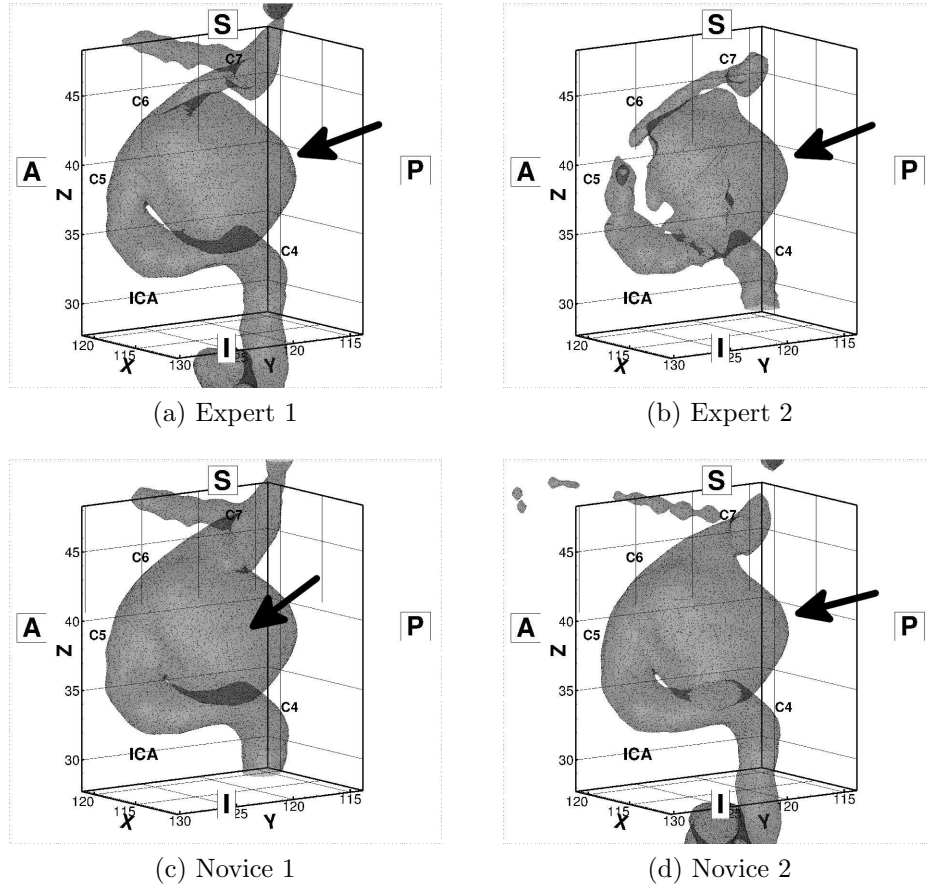
Figure 2.8: This aneurysm was not available for analysis due to several factors. The aneurysm contacts the vessel wall at several locations other than the neck, creating surface reconstruction challenges. Also, the neck can be interpreted to progress along the inner curve of the ICA which prevents a cutting plane from reasonably decoupling the two geometries.

Modality	X/Y Resolution (mm)	Slice Spacing (mm)†	Slice Thickness (mm)
CTA	0.31	0.50	1.00
MRA	0.63	0.80	0.80
MRToF	0.43	1.00	1.00
Mean	0.46	0.77	0.93
Std	0.16	0.25	0.12
†: the slice spacing was computed as the magnitude of a normal vector between the first two adjacent slices			

Table 2.1: Phantom scan parameters

with an anterior communicating aneurysm was scanned using all three modalities at our institution and the images were used as the training set (2.1). This set was ideal for training purposes because the DICOM scans were in the three modalities, the images lacked significant artifacts locally to the vessels, the ratio of aneurysm maximimum diameter to vessel diameter was high, and the lumen geometry was available for the novices to inspect and compare with.

2 .2.2.2 Development

To develop our protocol, we standardized VMTK script pipelines used in segmentation and mesh generation. Two experts segmented the development set using the protocol and the segmentations were compared qualitatively by the two experts and a third observer. From this comparison, changes were made to refine the instructions given to the user for segmentation. Next, we examined segmentations that had unique image or segmentation challenges and developed a process tree to

Patient	X/Y Resolution (mm)	Slice Spacing† (mm)	Slice Thickness (mm)	Average Aneurysm Height (mm)
1	0.39	0.60	0.60	2.49
2	0.39	0.70	0.70	3.33
3	0.27	0.45	0.90	3.12
4	0.43	1.25	1.25	2.09
5	0.35	0.60	1.20	1.10
6	0.31	1.00	1.00	1.50
Mean (mm)	0.36	0.77	0.94	2.27
Std (mm)	0.06	0.30	0.26	0.88
†: the slice spacing was computed as the magnitude of a normal vector between the first two adjacent slices				

Table 2.2: Study Population: scan parameters

handle such events.

2 .2.2.3   Testing

To test the effectiveness of our protocol, we evaluated the variation of between classes of users. Zou *et al.*   investigated the accuracy of tumor segmentation between medical students manual segmentations with and without training [64]. They found improved agreement after training from an expert segmenter. Since our method uses a semi-automatic segmentation method, we opted to train novices on phantom training data with a written protocol. Novice users were given training on the protocol consisting of some background on the algorithms used in VMTK, models and diagrams of the intercranial vasculature anatomy, and examples of how to identify vessels in DICOM image data. The training set was used to familiarize the novice operators on the protocol and the nature of the data to be segmented.

Two trained novices and two experts were given the testing set from our patient database to segment using the protocol. All users were given the aneurysm location as identified by the clinician. From the final meshes, the aneurysms were extracted from the total geometry using a cutting plane. The placement of the cutting plane was based on the location and orientation a surgical clip would be placed to operatively treat the aneurysm (Fig. 2.9). Each seperation plane was determined independently to avoid plane reproduction that was not geometry-based. From the resultant segmentations, aneurysm indices were computed using in-house code [33, 46].

We examined the effect of aneurysm shape indices due to the placement and orientation of the final cutting plane on a basilar aneurysm with a poorly defined
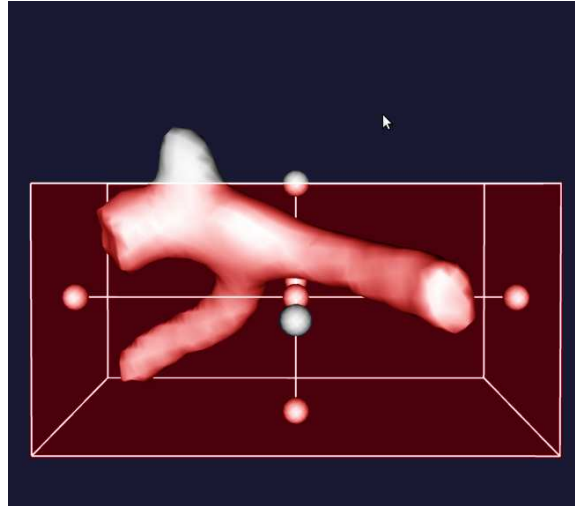
(a)
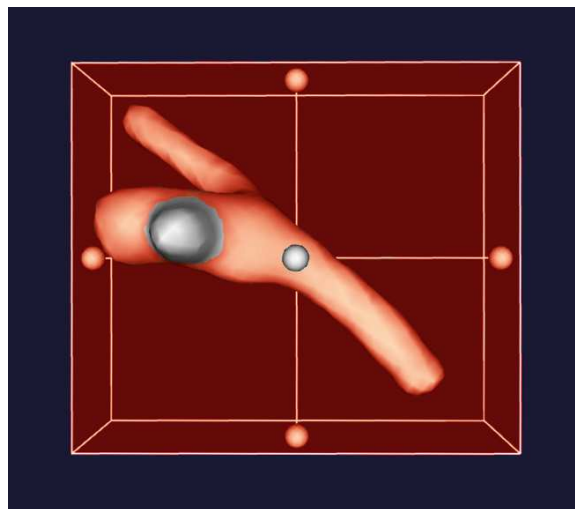
(b)

Figure 2.9: The cutting plane is chosen as if a surgical clip would be placed on the aneurysm.
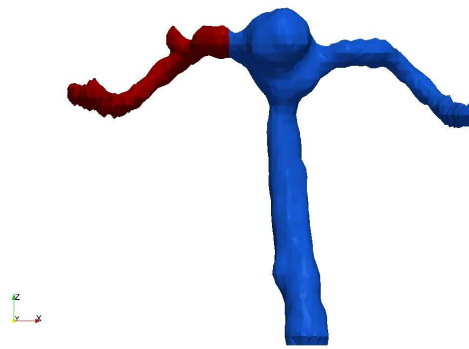
(a) First cut
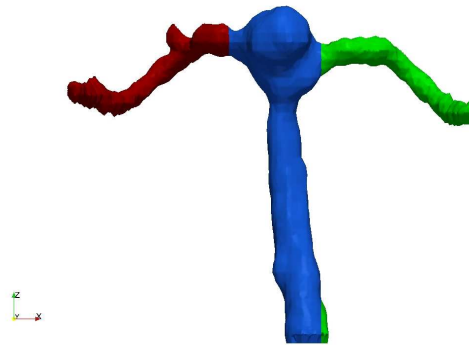
(b) Second cut
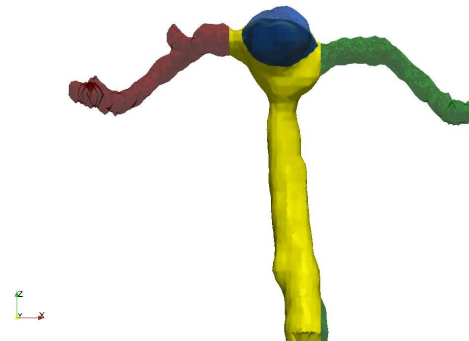
(c) Final cut
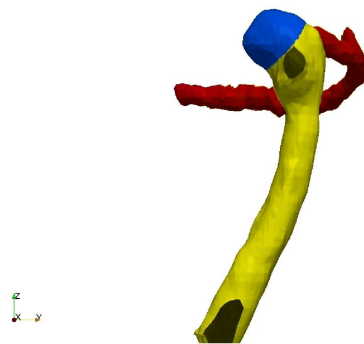
(d) Side view of final

Figure 2.10: Planes were used to decouple aneurysms from their parent vessels. a) The patient's left PComm is removed (red). b) The patient's right PComm is removed (green). c-d) Lastly, the basilar artery is removed (yellow), leaving the aneurysm geometry (blue). In d) the right PComm is not shown.

neck. Patient 2 had the largest clinically measured aneurysm (Table 2.2), manifesting itself as a dilation of the superior side of the intersection of the basilar with the Cirle of Willis. The dilation extends inferiorly along the basilar artery. As a result, its neck definition lends itself to the most interpretation. We examined the change in height by varying the height by 0.025 mm, up to 0.01 mm

2 .2.3   Evaluation

The geometric indices we use to evaluate user agreement are single and multi-dimensional. Table 2.3 summarizes the indices and metrics used to measure user variation. The 2- and 3-D indices have been developed and reported in Ma *et al.* [33] and Raghavan *et al.* [46], while the 1-D indices are the common clinical measures [56].

1-D Indices	
Height	$H = $ Euclidean distance from cutting plane to first farthest edge
Maximum Diameter	$D_{max} = $ Maximum diameter of the aneurysm
Maximum Neck Diameter	$D_{neck} = $ Maximum diameter in the cutting plane
2-D Indices	
Aspect Ratio	$AR = \frac{H}{D_{neck}}$
Bottleneck Factor	$BF = \frac{D_{max}}{D_{neck}}$
Bulge Location	$BL = \frac{H_{maxcross-section}}{H}$
3-D Indices	
Undulation Index	$UI = 1 - \frac{V}{V_{convexhull}}$
Ellipticity Index	$EI = 1 - (18\pi)^{1/3}(\frac{V^{2/3}}{S_{closedconvexhull}})$
Non-Sphericity Index	$NSI = 1 - (18\pi)^{1/3}(\frac{V^{2/3}}{S_{closed}})$

Table 2.3: Geometric Indices

CHAPTER 3
RESULTS

3 .1 Segmentations

Tables 3.1–3.4 show the segmentations from all four users. All segmentations were done on the same workstation.

3 .2 Index Plots

We compared indices between users of similar skill sets to qualitatively assess index agreement. The results are shown in figures 3.8–3.14. To analyze the agreement, we computed the linear regression slope constrained through the origin (Table 3.1), the Student's t-test (Table 3.2), as well as the coefficient of determination for unconstrained linear regression (Fig. 3.8 - 3.14).

3 .3 ANOVA

Since our testing set is a sampling from our larger patient database, an analysis of our data should include a measure of the variation within our testing set for the indices calculated. If the testing set consists of separate populations (e.g. spherical and oblong), ANOVA analysis can indicate if a particular patient's indices are outside the normal variation. This fact is also true for our segmenters: for example, if one segmenter produces aneurysms with indices outside the expected normal variation, an ANOVA test can indicate that. Finally, unlike Student's t-test, ANOVA gives a measure of the interaction between the two variables: patient and segmenter. Suppose novices segment spherical aneurysms with some bias, but experts segment

oblong aneurysms with a different bias. When the t-test is computed, the combined effect may produce a P-value that does not reflect the actual variation in the data.

Repeated measures ANOVA analysis (0.05 significance) was performed for both users and patients. The results are displayed in tables 3.3–3.4.

	Height	D_{max}	D_{neck}	AR	UI	EI	NSI
Experts	1.06	0.93	0.93	1.17	0.92	1.05	0.99
Novices	1.03	1.04	1.07	0.92	0.92	1.16	1.13
Means	1.03	0.91	0.9	1.13	0.71	0.93	0.91
Regression constrained through origin							

Table 3.1: Linear Regression Slopes for Indices

	Height	D_{max}	D_{neck}	AR	UI	EI	NSI
Experts	0.72	0.69	0.69	0.13	0.44	0.71	0.71
Novices	0.98	0.87	0.75	0.64	0.91	0.55	0.62
Means	0.97	0.62	0.56	0.4	0.18	0.78	0.6

Table 3.2: Student's t-test for Indices

	SS	MS	F	P-value
Height (mm)	0.72	0.14	0.62	0.69
Max Diameter (mm)	26.32	5.26	129.05	5.3e-10
Neck Diameter (mm)	26.06	5.21	84.80	6.2e-9
Aspect Ratio	0.32	0.06	11.44	3.1e-4
Undulation Index	0.01	1.4e-3	3.46	0.04
Elipticity Index	0.01	1.3e-3	10.28	5.2e-4
Nonsphericity Index	0.01	2.0e-3	9.75	6.6e-4
degrees of freedom $= 5, F_{critical} = 3.11$				

Table 3.3: Data set: ANOVA with replacement

Patient 1			
Resolution (mm)	Slice Spacing (mm)	Thickness (mm)	Aneurysm Height (mm)
0.39	0.60	0.60	2.49
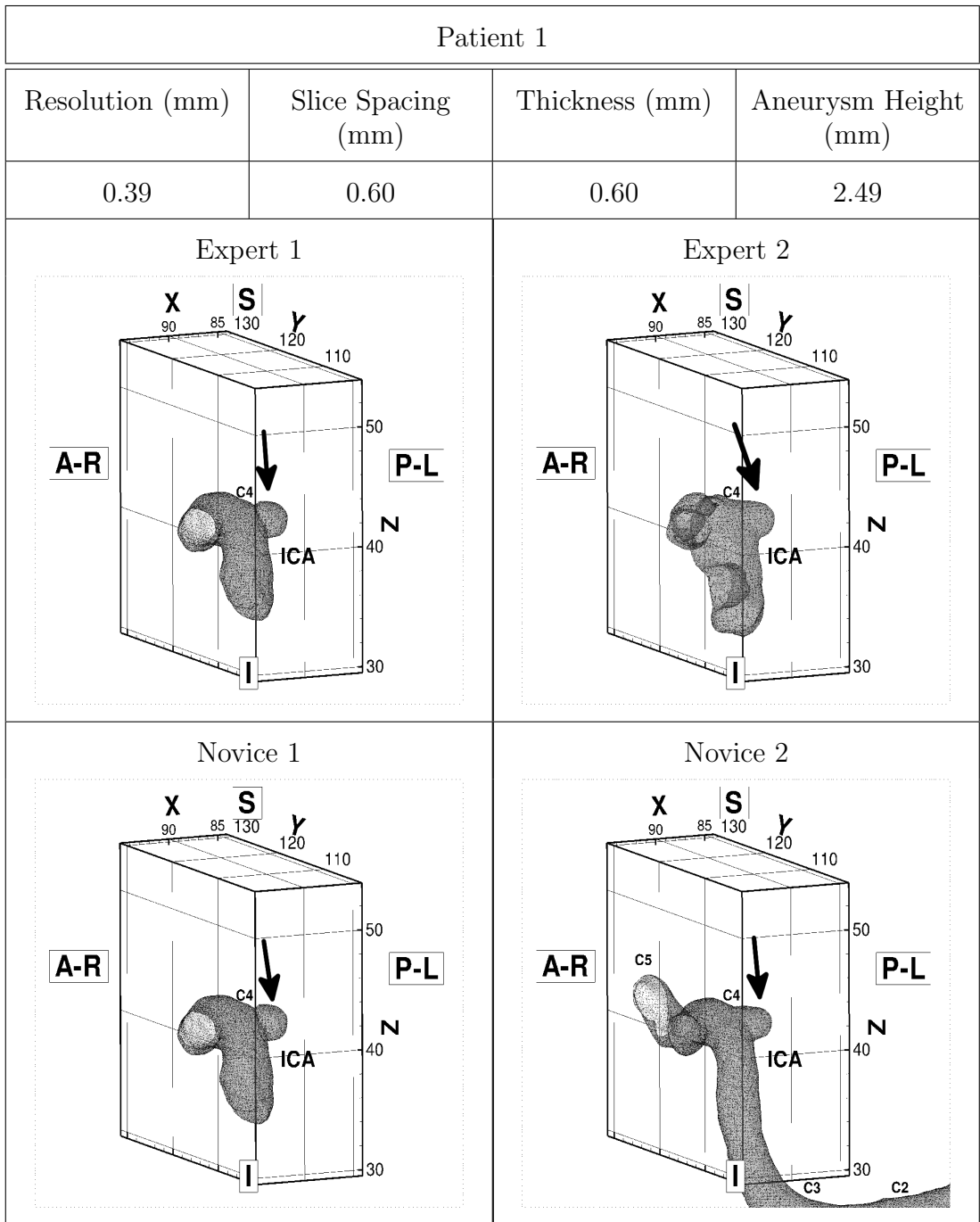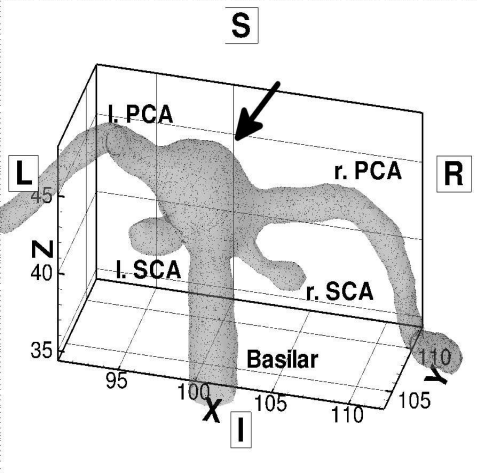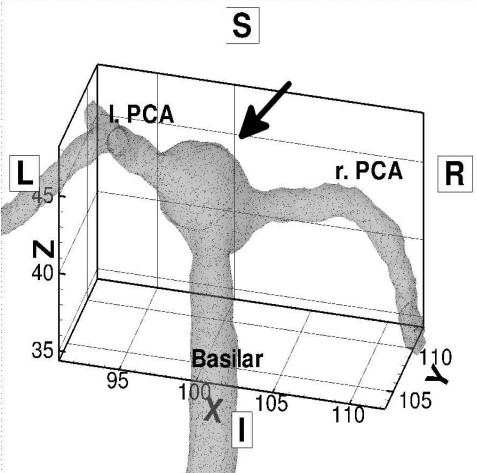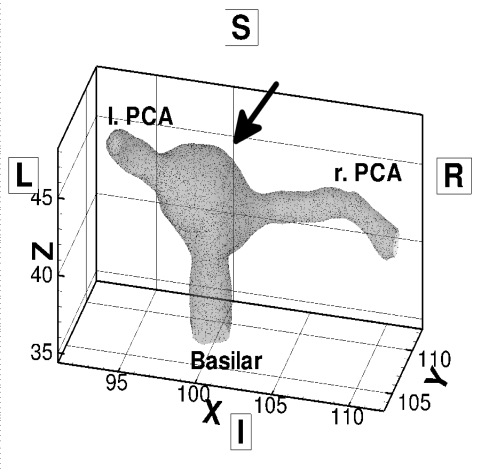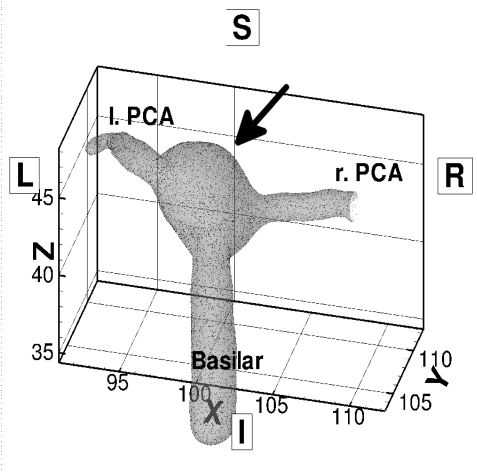
Figure 3.1: Patient 1

Patient 2			
Resolution (mm)	Slice Spacing (mm)	Thickness (mm)	Aneurysm Height (mm)
0.39	0.70	0.70	3.33

Expert 1

Expert 2

Novice 1

Novice 2

Figure 3.2: Patient 2

Patient 3			
Resolution (mm)	Slice Spacing (mm)	Thickness (mm)	Aneurysm Height (mm)
0.27	0.45	0.90	3.12

Figure 3.3: Patient 3

Patient 4			
Resolution (mm)	Slice Spacing (mm)	Thickness (mm)	Aneurysm Height (mm)
0.43	1.25	1.25	2.09
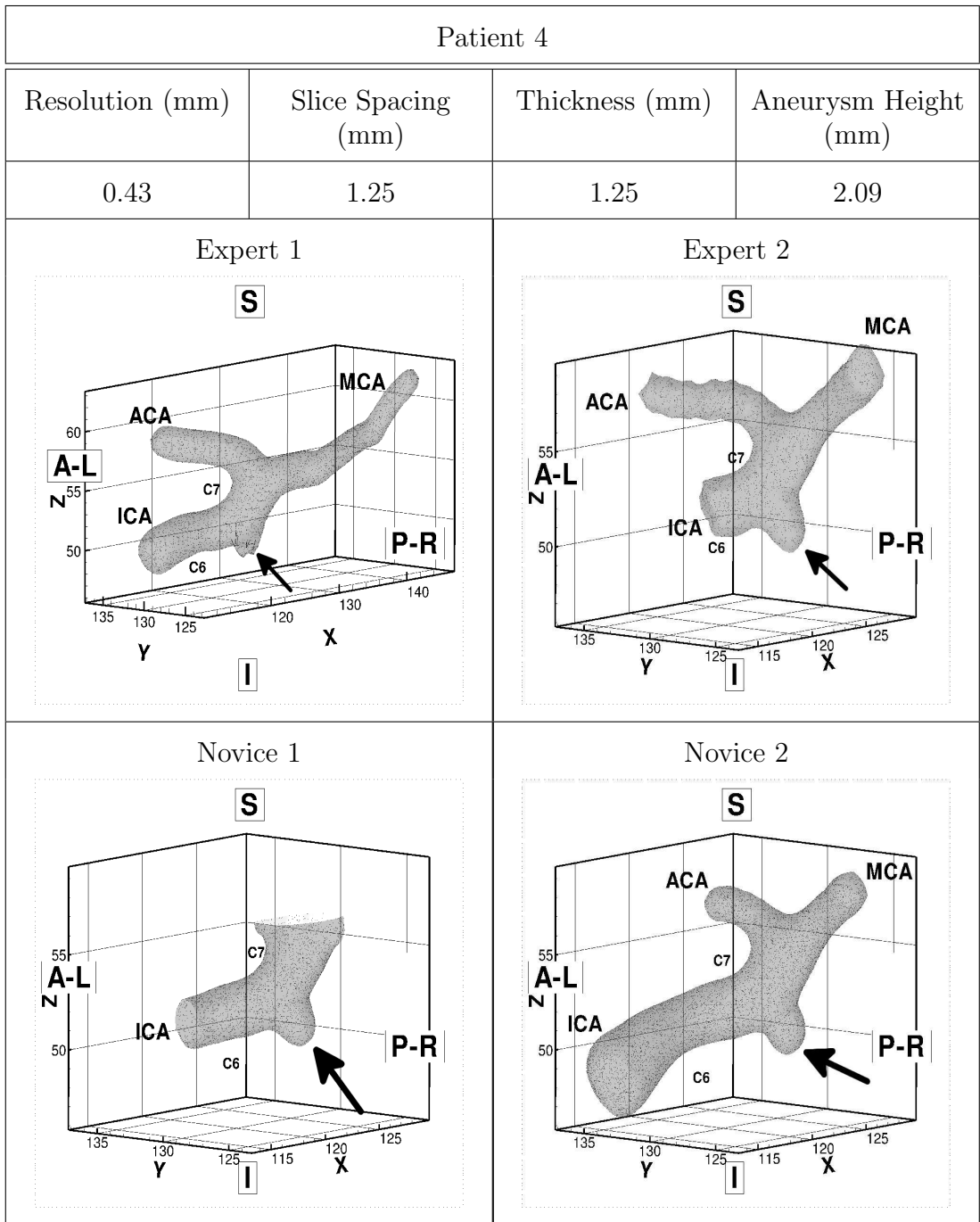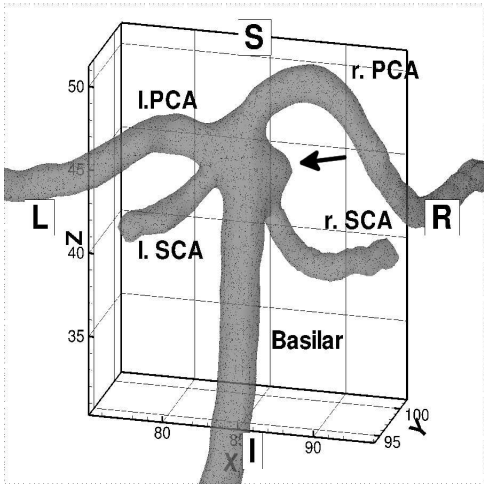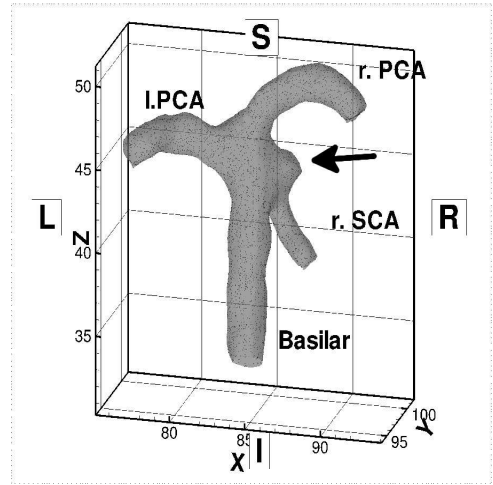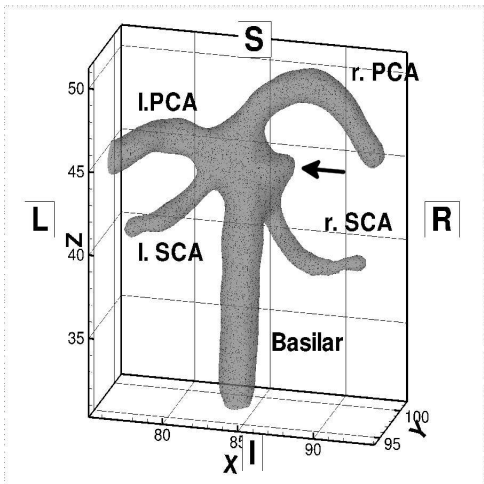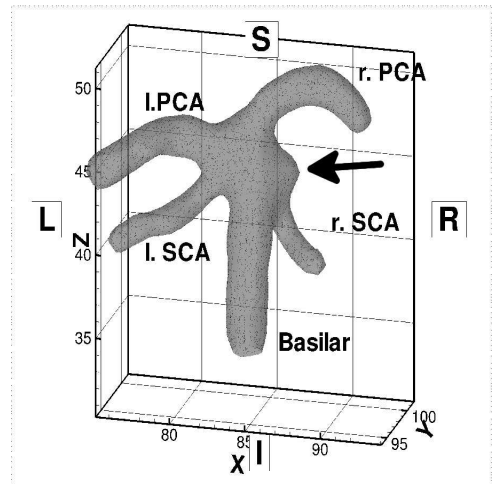
Figure 3.4: Patient 4

Patient 5			
Resolution (mm)	Slice Spacing (mm)	Thickness (mm)	Aneurysm Height (mm)
0.35	0.60	1.20	1.10

Figure 3.5: Patient 5

Patient 6			
Resolution (mm)	Slice Spacing (mm)	Thickness (mm)	Aneurysm Height (mm)
0.31	1.00	1.00	1.50

Figure 3.6: Patient 6

Figure 3.7: Expert 2 Segmentation of Subject 3: the circled geometry is the indentation due to the anterior clinoid process (scale in mm).
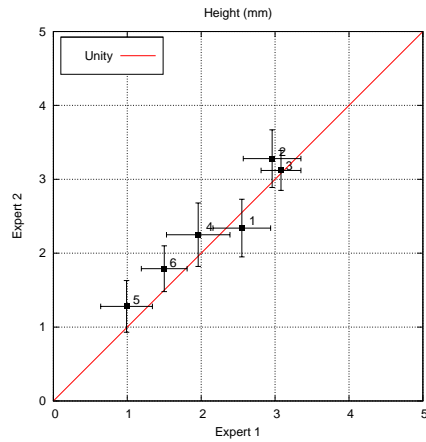
(a) Experts
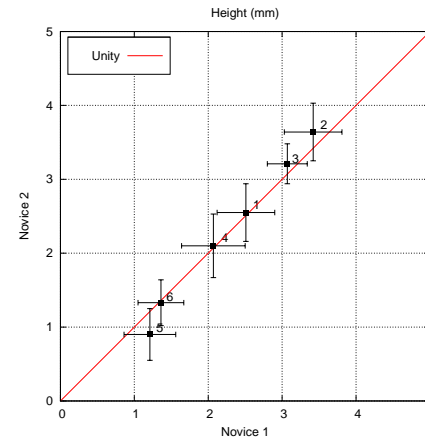
(b) Novices
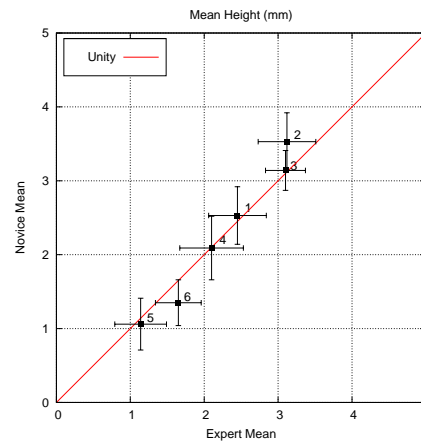
(c) Means

Figure 3.8: Comparison of Height Measurements (error bars equivalent to x/y resolution for image)
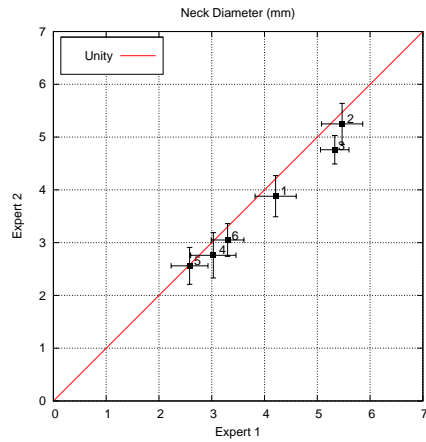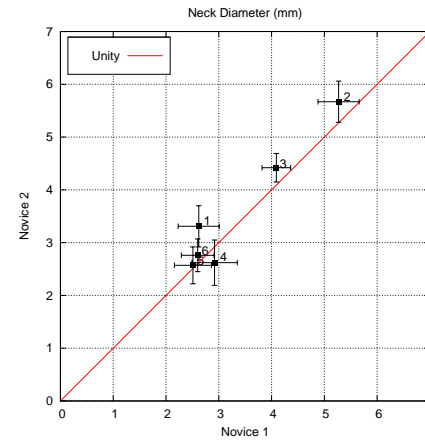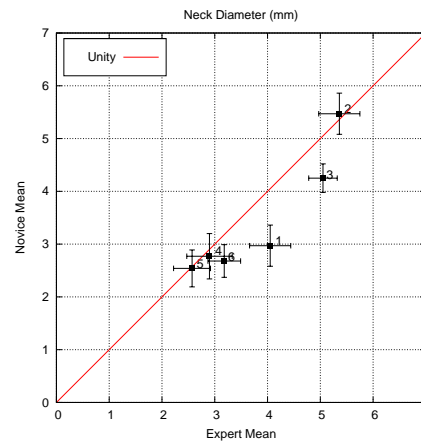
(a) Experts

(b) Novices

(c) Means

Figure 3.9: Comparison of Neck Diameter Measurements (error bars equivalent to x/y resolution for image)
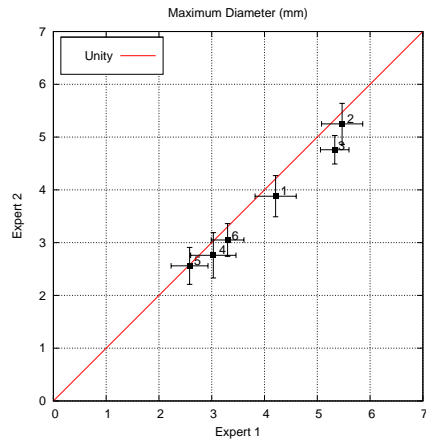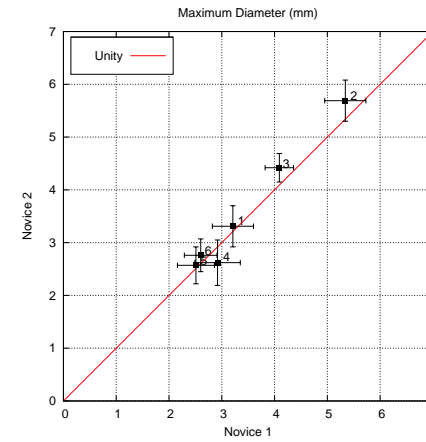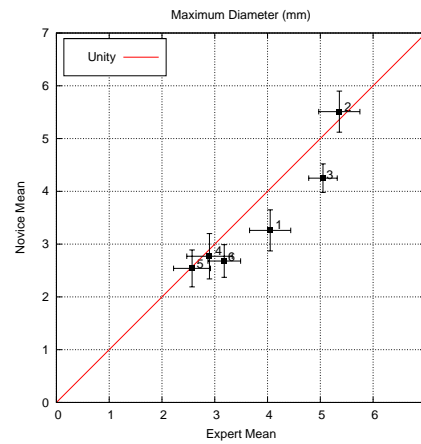
(a) Experts

(b) Novices

(c) Means

Figure 3.10: Comparison of Maximum Diameter Measurements (error bars equivalent to x/y resolution for image)
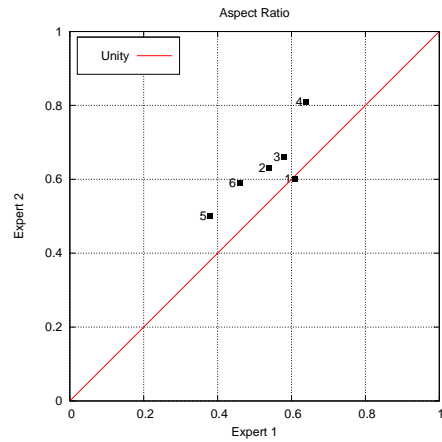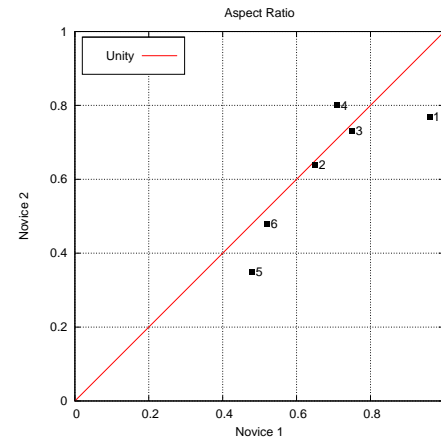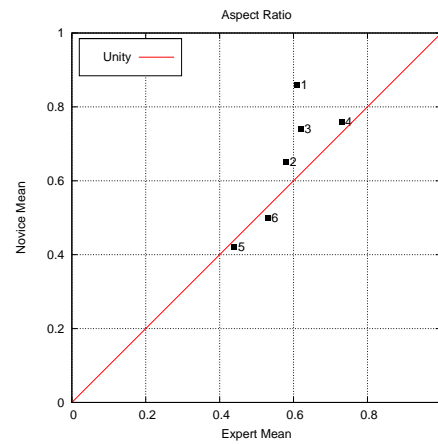
(a) Experts

(b) Novices

(c) Means

Figure 3.11: Comparison of Aspect Ratio
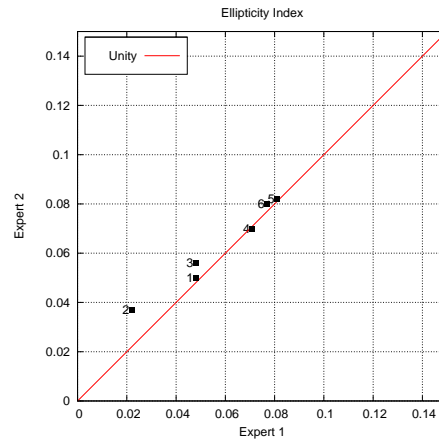
(a) Experts
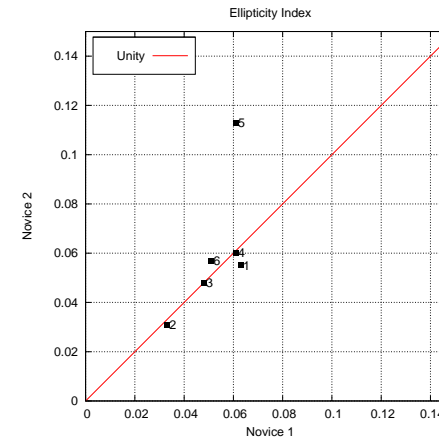
(b) Novices
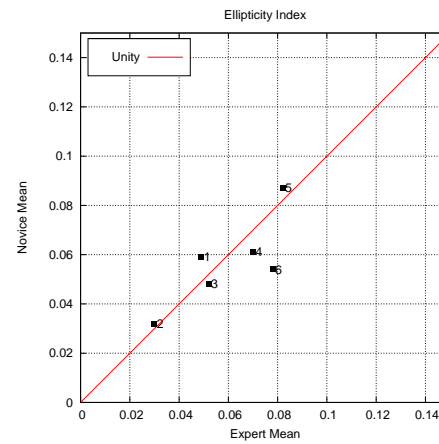
(c) Means

Figure 3.12: Comparison of Ellipticity Index
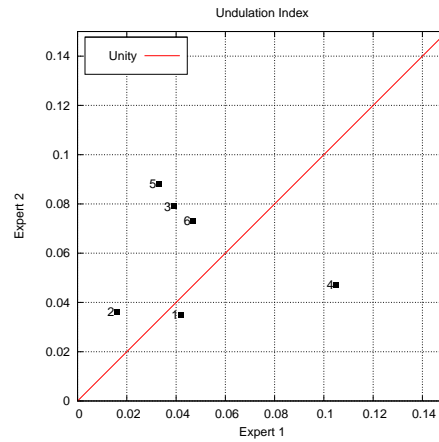
(a) Experts
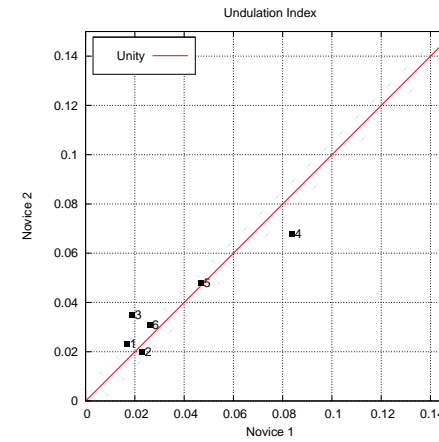
(b) Novices
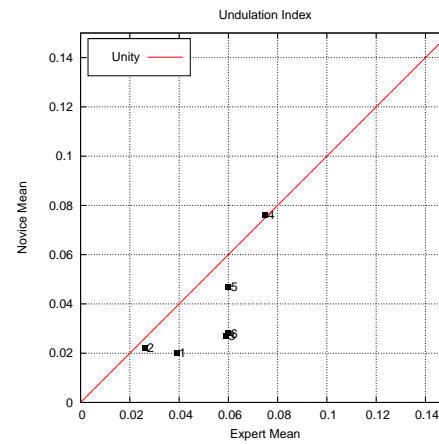
(c) Means

Figure 3.13: Comparison of Undulation Index
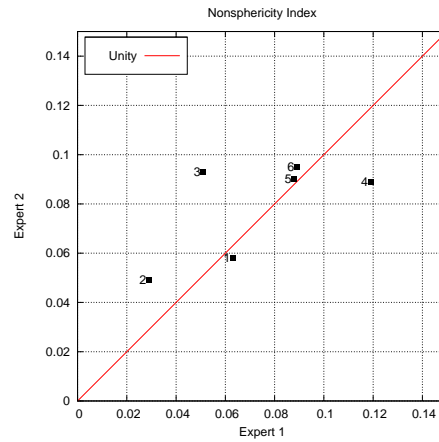
(a) Experts
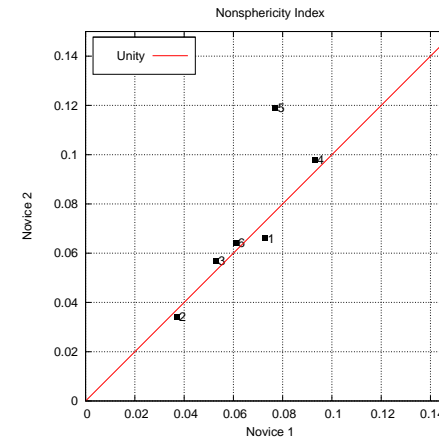
(b) Novices
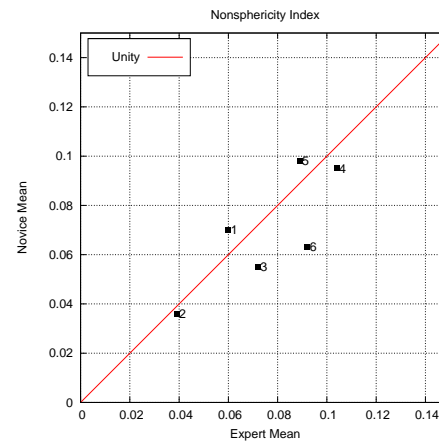
(c) Means

Figure 3.14: Comparison of Nonsphericity Index

	SS	MS	F	P-value
Height (mm)	11.33	11.33	48.54	1.5e-5
Max Diameter (mm)	0.72	0.72	17.65	1.2e-3
Neck Diameter (mm)	0.97	0.97	15.81	1.8e-3
Aspect Ratio	0.03	0.03	5.22	0.04
Undulation Index	1.6e-3	1.6e-3	4.12	0.07
Elipticity Index	5.9e-5	5.9e-5	0.47	0.51
Nonsphericity Index	2.6e-4	2.6e-4	1.25	0.29
degrees of freedom = 1, $F_{critical} = 4.75$				

Table 3.4: Users: ANOVA with replacement

CHAPTER 4
DISCUSSION

4 .1   1-D Indices

4 .1.1   Height

Height measurements between users showed strong relationship in both r^2 for expert ($P = 0.94$), novice ($P = 0.99$), means ($P = 0.97$), and in ANOVA ($P = 1.5e - 5$). Within the testing data, ANOVA could not find a significant similarity between patient heights. This result might hint that our protocol is robust enough to handle a wider range of aneurysm sizes and still return a height measurement with accuracy.

4 .1.2   Diameter Measures

Neck and maximum diameter indices showed similar variation and P-values for all measures (Tables 3.2, 3.4, Figures 3.9, 3.10). Our diameter measures are closely related, since many small aneurysms do not present a concave neck border. Therefore, when we decouple the aneurysm from the vessel, we can define an aneurysm 'skirt' - a region of the lumen that can be considered in transition between the vessel and the aneurysm. For aneurysms with a bulge-like geometry, the maximum diameter is often equal to the neck diameter at or near the edge of the skirt.

4 .2   2-D Indices

4 .2.1   Aspect Ratio

The aspect ratio (AR) index shows a decrease in the r^2 values compared to the 1-D indices it is computed from figure 3.11. For experts, AR suffers from the resolution available for small aneurysms: Expert 1 overestimated neck diameters compared to Expert 2 and the reverse was true for height. Both interpretations are valid in the resolution scales we encountered. In figure 3.11b, the novice segmentations of Patient 1 shows noticeable disagreement between novice users due to Novice 1 segmenting a strongly concave neck for Patient 1. In the comparison of AR means, subject 1 is still an outlier.

4 .2.2   Ellipticity Index

The ellipticity index (EI) values for experts and novices show strong agreement (Fig. 3.12) for r^2 and Student's t-test. Novices suffer lower confidence due to the segmentation of Patient 5. This is a SCA aneurysm with a high SNR for the ROI and one would anticipate good agreement. If we examine the images in Tables 3.3 and 3.4, we can see that Novice 1 segments a steeper aneurysm than Novice 2's. The EI is specifically designed to capture this difference in geometry.

4 .2.3   Undulation Index

The novice comparison shows good agreement between the users ($r^2 = 0.90, P = 1.173 - 3$). The experts varied the greatest within this index, with $r^2 = 0.02$ ($P = 7.87e - 1$). On closer examination, this disagreement was due to many factors.

Patient 4 could be explained by a poor mesh generated by Expert 1 (Fig. 3.1). In addition, this aneurysm was directed towards the tip of the anterior clinoid process of the sphenoid bone. Expert 2 interpreted the aneurysm deforming around the anterior clinoid process of the sphenoid bone (Fig. 3.7), while the other three segmented the aneurysm as projecting towards the bone, but not in contact.

The disagreement in Patients 5 and 6 could not be determined, but it is hypothesized that the skirts of these aneurysms created a disparity between the volume of the aneurysm and it's convex hull. Patient 3's UI index for both experts could not be explained.

4 .2.4 Nonsphericity Index

For NSI, Expert 2 produced a 'long' aneurysm for Patient 3. Novice 2 segmented a 'flat' aneurysm compared with the other segmenters (Fig. 3.14). The NSI index is shown to capture these differences.

CHAPTER 5
CONCLUSION

The sensitivity of segmented brain aneurysms to users was studied. Six aneurysms were used for user sensitivity analysis. 1-D indices showed significant agreement between users and patients, within the resolution ranges of the source images. Aspect ratio was more sensitive to variations between height and neck diameter, which displayed systematic variation between experts.

Small aneurysms present a significant challenge for clinical evaluation due to partial volume effects and grey-scale value interpretations [3, 5]. The choice of clipping plane for the aneurysms also has a strong influence to these measures and therefore we expect more volatility in this comparison. If we consider the additional influence that the cutting plane adds to our measurements in 1-D, the disagreement between users is expected.

Bottleneck factor (BF) and bulge location (BL) were both found to be trivial measures for our group of small aneurysms. The aneurysms that were segmented successfully from our initial testing set (6 of 10) where all 'dome-like' geometries. These aneurysms neck diameters are roughly equvalent to the maximum diameters. It is possible that the current resolution limitations in clinical scanners make BF and BL inappreciatable for aneurysms of this size.

3-D indices displayed mixed results for novices and experts. While experts showed strong agreement in EI, they varied more with UI and NSI. Novices were the exact opposite. Qualitatively, examining each patient's segmentations overlayed showed surface deviations between the four segmenters, but the overall shape of the aneurysms was consistent to the naked eye. One noticable exception was subject

3, previously discussed (Sec. 4 .2.3). The increased f-value of our UI (Table 3.4) reflects this abnormality. Interpretation of images is, therefore, still an important aspect of computer-aided segmentation protocols like ours and care needs to be taken among presenters to note alternative surface interpretations and nearby structures.

Our protocol brings together many techincal aspects of file handling, image segmentation, and mesh creation into a user-friendly process that increases investigation startup, segmentation throughput and surface reproducibility. Based on user sensitivity analysis, we did not find a statistically significant difference between the average expert's segmentation geometry and that of the average novice. However, lack of significant difference does not necessarily suggest that novice segmentations are as effective as experts. Indeed, as noted by the results, some indices do differ at a measureable level between and among novice and expert. These differences may be due to the choice of the cutting plane used to isolate the aneurysm sac and may be addressed by developing a consistent method for sac isolation and further user sensitivity studies.

APPENDIX A
SELECTED VMTK ALGORITHMS

A.1 Colliding Fronts Algorithm

The Colliding Fronts method is a specific application of the Fast Marching method, used in our protocol to segment spherical shapes. The user selects two starting points, p_1 and p_2 to begin with. Two wavefronts,

$$|\nabla T_1| = \frac{1}{1+I}$$

and

$$|\nabla T_2| = \frac{1}{1+I}$$

corresponding to the eikonal equations for each point are propagated using the Fast Marching algorithm described in A.2. The resulting volume is defined as all voxels where

$$\nabla T_1 \cdot \nabla T_2 < 0.$$

The cylindrical nature of this segmentation becomes apparent as one considers this method as a minimum path solution between the two points, with the wave nature of the Fast Marching solutions performing a diffusion on the minimum path.

A.2 Fast Marching Algorithm

To solve the equation $|\nabla T|F = 1$ described in Sethian [53], VMTK makes use of the Fast Marching method. The user selects a starting source voxel and the travel time to surrounding (trial) voxels is calculated as a function of voxel intensity. This is done analytically to reduce some first-order numerical errors. An array of the travel times for the trial voxels is sorted from minimum to maximum, representing the wave front of the surface. The voxel with minimum trial time is added to the known array. The known voxels constitute the volume of the aneurysm and the

trial is

$$\frac{1}{F_{ijk}} = \left(\begin{matrix} max(D_{ijk}^{-x}T, -D_{ijk}^{+x}T, 0)^2 + \\ max(D_{ijk}^{-y}T, -D_{ijk}^{+y}T, 0)^2 + \\ max(D_{ijk}^{-z}T, -D_{ijk}^{+z}T, 0)^2 \end{matrix} \right)^{1/2}$$

where

$$D_{ijk}^{+\phi}T = \frac{T(\phi + h, t) - T(\phi, t)}{h}$$

and

$$D_{ijk}^{-\phi}T = \frac{T(\phi, t) - T(\phi - h, t)}{h}$$

are first order linear wave equation schemes. As the trial array updates, the list of wavefront voxels grows as the wave propagates. At each update, the known array keeps the voxel with minimum travel time at each evaluation of the wavefront to the array. The known points are used to recalculate the times of the trial voxels. The algorithm terminates when the minimum travel time within the trial array is greater than the stopping value set in VMTK.

From Sethian:

1. Begin loop: Let A be the $Trial$ point with the smallest T value.

2. Add the point A to $Known$; remove from $Trial$.

3. Tag as $Trial$ all neighbors of A that are not $Known$. If neighbor is more than one grid point away, remove and add to the set $Trial$.

4. Recompute the values of I at all $Trial$ neighbors of A according to our update equation by solving the quadradic equation.

5. Return to top of loop.

A.3 Level Sets Equation

Given a surface Γ in $\Re^n$, there exists a hypersurface Ψ in $\Re^{n+1}$ such that the propagation of Γ normal to its surface is an n-dimensional sample of Ψ that solves the equation

$$|\nabla \Gamma| F = 1$$

, where F is the speed function of the surface propagated.
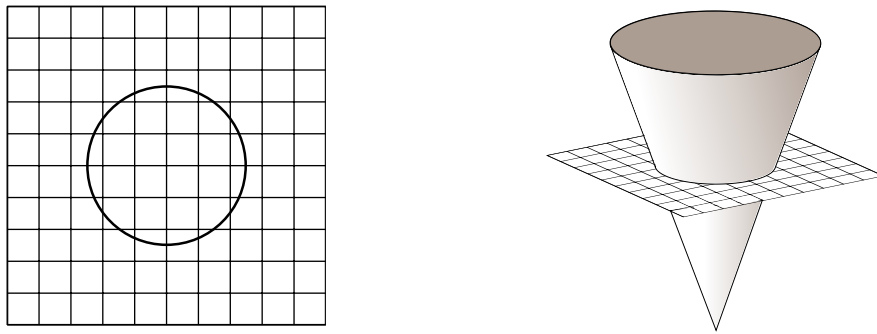
Figure A.1: Consider the image on the left as the initial space $\Re^2$ with a surface Γ. The image on the right is the $\Re^3$ space, where Γ can be represented as Ψ. As Ψ moves perpendicular to the plane, the surface Γ in $\Re^2$ space is perceived as expanding or contracting. If Ψ develops abnormalities, the surface in $\Re^2$ can become more complex.

This amounts to treating the surface as a continuous function (as opposed to a discrete function of qualifying grid points), allowing shocks and merges on the surface to be computed with improved ease and speed.

A.4 Marching Cubes Algorithm

Marching Cubes is a sequential-transversal isosurface extraction method first described by Lorensen and Cline [32]. It seeks to define a $\Re^3$ surface of some scalar α in a scalar field. Since the value α is not guaranteed to exist for any voxel within

the $\Re^3$ space, Marching Cubes interpolates for the value α between grid points using linear interpolation. The interpolation points between any two vertices needs only to be computed once, after which it can be reused for the three remaining cubes with the same two vertices.

Marching Cubes defines cubes of data space consisting of eight vertices V_i, where each V is a voxel intensity from the DICOM images. Marching Cubes searches all the cubes and stores the cubes that have one or more vertices with intensity $I \geq \alpha$. There are $2^8(256)$ different marked/unmarked vertex combinations, but this can be reduced by rotational and reflective symmetry to unique cases, displayed in Fig. A.2. Using mirror symmetry, we can further reduce the number of cases to 14.
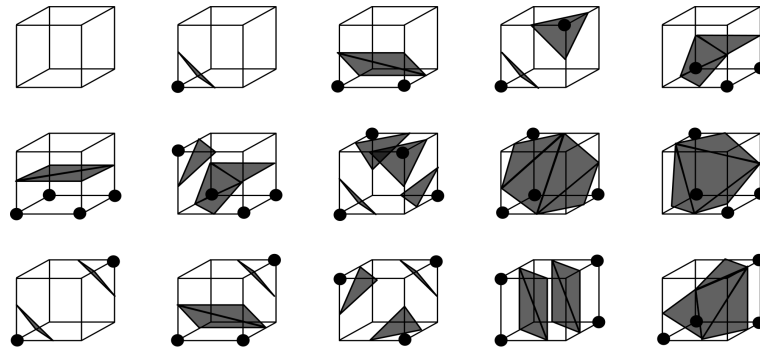
Figure A.2: The fifteen unique cases for Marching Cubes cube/isosurface intersection. Note that case 10 and 15 can be further combined using mirror symmetry. (Cases are numbered left to right, top to bottom)

Having identified the cubes of interest, Marching Cubes uses the lookup table describing the 14 cases to determine which cases apply to each cube. In some instances, a cube may have more than one case, in which the surrounding cubes are used to decide which case will result in a complete surface (i.e. a surface without a hole at the cube in question).

APPENDIX B
SUPPLEMENTAL MATERIAL

B.1   Protocol Manual

Aneurysm Reconstruction Protocol (v. 4.1)

Selecting 3D Series

1. Before running the reconstruction script, find the location of the aneurysm from the database.

2. Open a terminal and run:

   `$ aneurysm_bash_script.sh`

3. In the first window, select the destination folder (ex./home/user/Desktop/-1009/CD#/yourname). *This is the location that all subsequent files will be saved..*

   > CAUTION: If you wish to reconstruct a DICOM series other than the primary series from a CD, create an alternate folder in .../####-/CD#/ named after your DICOM series (ex. for DICOM folder SR0034 would be .../####/CD#/SR0034/) and select that folder as your patient folder. **This will prevent file overwriting!**

4. If the DICOM series has not been read before, you will need to select the root DICOM folder for that series.   (If it has been read, there will be a ####_all.vti file: skip to step 2.0)

   (a) MIPAV will open automatically and allow you to browse the DICOM folder for the series you want to segment. Once identified, note the number of files in the folder and close MIPAV.

(b) In the next dialog, select the DICOM folder that has the series you identified. Currently, the best way is to find the folder with the right number of files.

(c) Click "Okay." This will create a file "####_all.vti" file for that DICOM series, where ### is the patient ID number you previously entered.

WARNING: This file, if placed in the .../####/CD#/ folder is assumed to be the primary DICOM series scan for that scan date! If you wish to reconstruct an alternate series for that date, follow the CAUTION statement in step 3.

Creating Volumes

1. You will be asked for how many aneurysms for this patient. If you don't know the number, create a Circle of Willis (CoW) VOI and examine the data during that process, then rerun the code when finished. (See step 2.2)

   (a) If running this code for multiple aneurysms, select them in the alphebetical order of their position so to maintain consistant numbering between users. (A left side aneurysm is before a right side aneurysm at the same location.) If you make a mistake, you can manually rename all the resulting files later by running these commands on the folder:
   ```
   $ mv 1001_2_AComm_* 1001_1_AComm_*
   $ mv 1001_1_PComm_right_* 1001_2_PComm_left_*
   ```
   Example for renaming all AComm files for patient 3010 from aneurysm number two to number one and all left PComm files from one to two

2. For all patients, you should select the Circle of Willis (CoW) volume of interest (VOI) even if you don't intend on segmenting it. This is a special file and

should always be done first so that you can peek at the data and get some idea where you'd like to create your aneurysm VOI(s).
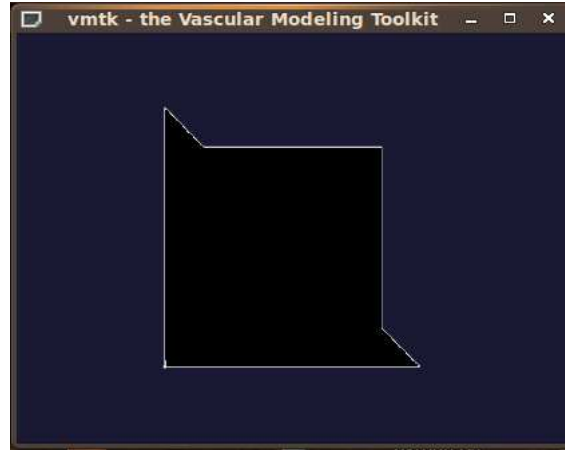
Figure B.1: VMTK render window

3. A VMTK render window will open. In the VMTK window, press "i" and a box will show up within the DICOM series. To move the planes of the box (expand or contract), click the toggle spheres in the center of the plane. When they turn red, move the mouse to adjust the plane position.

4. The CoW VOI is more standardized and should be created along the following guidelines. Should the aneurysm(s) fall outside this area, expand your CoW VOI to include them. If you are selecting any area other than the CoW, skip to Segmentation.

(a) Using the saggital plane, find where the ACAs branch past the A2 proximal segment and select the superior plane and the anterior plane.

Mouse Controls		
Button Action	Within Volume	Outside Volume
Left click	Display coordinates and HU value for voxel	Trackball rotation of volume
Scroll wheel rotation	Zooms in or out	Zooms in or out
Middle click	*Within blue borders (appears on click)*: progression through slices by image plane	Move volume within the rendered window
	Between blue border and green edge border (appears on click): Tilt image plane	
Right click	Adjust brightness (y-axis movement) and contrast (x-axis movement)	Zoom in or out

Quick keys	
r	center image
w	turn on surface triangles (turn off image)
s	turn on image (turn off triangles)
i	turn on interactor
q or e	quit (interactor, active render interaction, window, etc.)
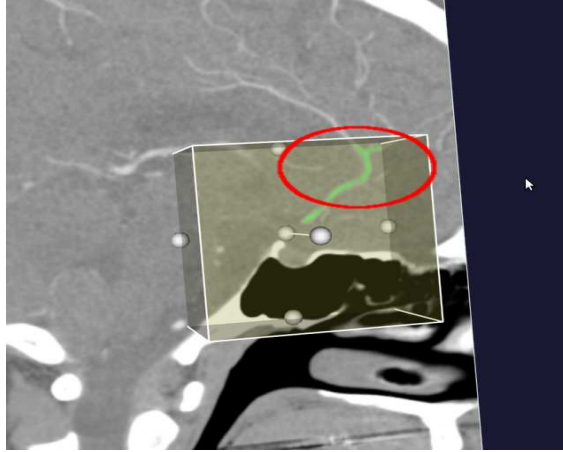
Figure B.2: ACA with A2 segment in green (patient facing right)

(b) Select the posterior plane from the location of the base of the basilar (where the vertebral arteries join together)
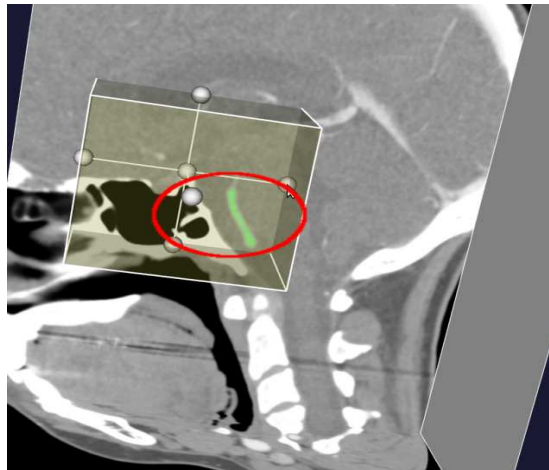
Figure B.3: Basilar highlighted in saggital plane (patient facing left)

(c) Select the inferior plane from one of the entry of the carotids into the base of the skull

Figure B.4: Carotid highlighted in green(patient facing right)

(d) Use the coronal plane to select the saggital planes past the branching of the MCAs on either side
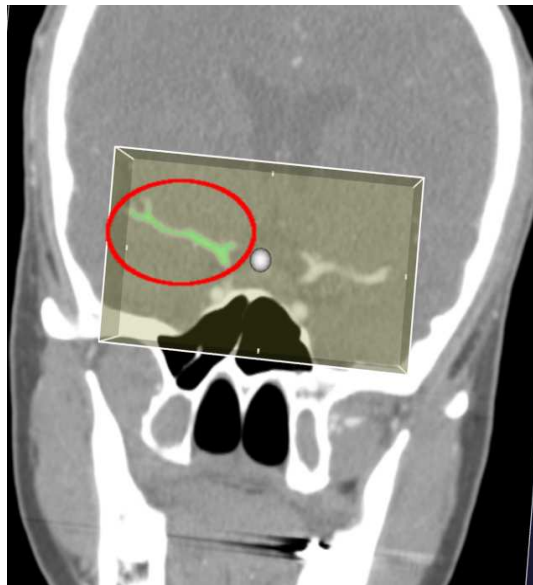
Figure B.5: Selecting the MCA (highlighted in green) past the bifurcation/trifurcation (patient facing out of page)

5. Once VOI is created, you will be asked if you want to segment it. (For CoW, this is a lengthy process and for now is not required.)

Segmentation

Note: When interacting with the visualization window, you must type 'q' to quit the interaction and move on to the next step in the segmentation

Note: VMTK merges segmentations together into a segmentation file. When the first acceptable segmentation is achieved, the user must select the merge option in order to save the segmentation. In essence, VMTK is asking if the user wants to merge that segmentation with the empty file and save it. All segmentations should be merged together unless a segmentation includes volume that is not part of the arteries.

1. Segment vessels first and aneurysm(s) last.

   Note for CTA data: air and bone segmentation may be needed and you will be asked if you'd like to include them in your segmentation. Use the isosurface option to segment the structures with smoothing parameters 300 0 0 1. For ICA locations, this is *highly recommended*.

2. **For vessel**: use colliding fronts method to segment vessels. Segment large vessels first and go on to the next step. Small vessels should be segmented after evolving the larger model. The following guidelines will be helpful in segmentation:

   (a) After selecting colliding fronts in the terminal window, input the upper and lower thresholds for the segmentation. This is an iteritive process and these values can be changed depending on the characteristics of the

local region of segmentation. For instance, an upper threshold may be necessary for a region of the VOI where the bone is close to the vessel, but that value may be inappropriate or unneeded elsewhere.

(b) Next, create two seed points by holding the Ctrl key and clicking on one of the planes at the point of intersection with a vessel. This is generally the geometric center of the vessel, but in segmentations near bone, points located furthest from the bone are more appropriate. When finished, type "q" in the render window.

(c) The resulting segmentation segment will be displayed. Examine this for errors or deficiencies in the segmentation by passing the planes through the surface from multiple angles and orientations. When you've completed your examination, type "q" in the render window.

(d) You will be asked in the terminal if you wish to accept this segmentation.

- <u>Decline</u>: if the surface includes volume ***that is not vessel*** (bone, partial volume effect, noise, etc.)

- <u>Accept</u>: if the surface includes a partial segmentation. (See the method for segmenting geometries with tight curves below.)

For geometries with tight curves ($> 90^o$): segmentation should be verified by passing the plane(s) orthogonal to the vessel at the curve. If some of the vessel geometry is excluded, add to the segment of the vessel curve by selecting seed points on the outside of the curve in conjunction with the already segmented inside of the curve. This should provide additional vessel capture at these bends (Fig. B.6).

3. **For the aneurysm**: use fast marching method to segment. The aneurysm
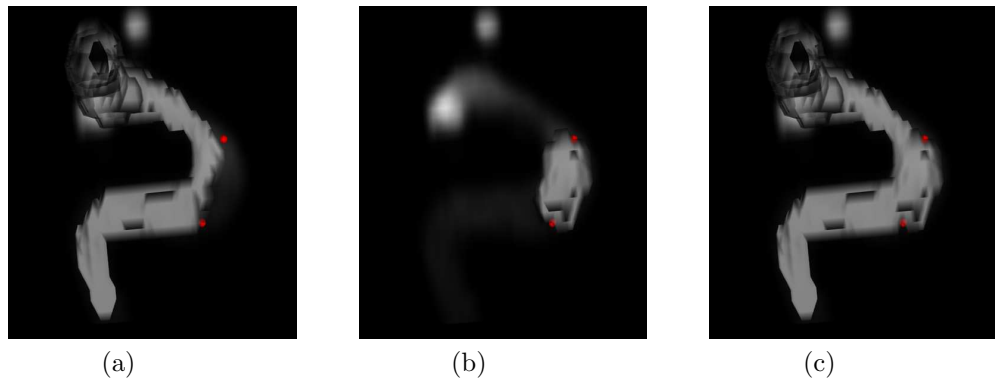
Figure B.6: (a) Sub-optimal segmentation with the ICA rim missing, (b) supplemental segmentation capturing the missing geometry, (c) the composite segmentation

segmentation and evolution will occur seperately from the vessels. Do not adjust the curvature scaling unless all other attempts to segment fail. The following guidelines will be helpful:

(a) Choose the source point in the center of the aneurysm.

(b) Move the planes so that they intersect the widest diameters in the cardinal planes. Select the target points at the edge maximums in the planes and any daughter sacs that might be otherwise missed.

(c) If you find that the aneurysm lays on a vessel such that the surface merges the aneurysm to the vessel outside the aneruysm neck, retry segmenting until the aneurysm no longer bleeds into the unwanted vessel (consider moving source point, changing thresholds, segmenting aneurysm in pieces, etc.)

4. Once the current initial segmentation step is complete, you will be prompted

in the terminal window:
```
Please input parameters (type return to accept current values,
'e' to end, 'q' to quit):  NumberOfIterations(0) Propagation
Scaling(0.0) CurvatureScaling(0.0) AdvectionScaling(1.0)
```

5. Enter the values seperated by spaces.

   - Iterations are always 300 for large vessels. Iterations can be adjusted for aneurysms and small vessels between 100-500.

   - Propogation controls radius expansion and should begin at 0

   - Curvature controls the erosion and dilation of vessels and should begin at 0

   - Advection controls the surface attraction to high gradients and should always be 1

6. After finding the surface that reflects a reasonable geometry (from image information and normal patient variabilities) you can repeat step 3 for smaller vessels.

7. Once completed, you will be asked for a shrinkage term for both aneurysm and vessel. Choose a positive number between 0 and 1. When the aneurysm no longer merges inappropriately with the vessel, confirm merge vessels and exit.

8. Finally, select the file ending in "combined_segm.vti" when prompted for a file to mesh. A tecplot file of the surface will be output.

B.2 Flowchart
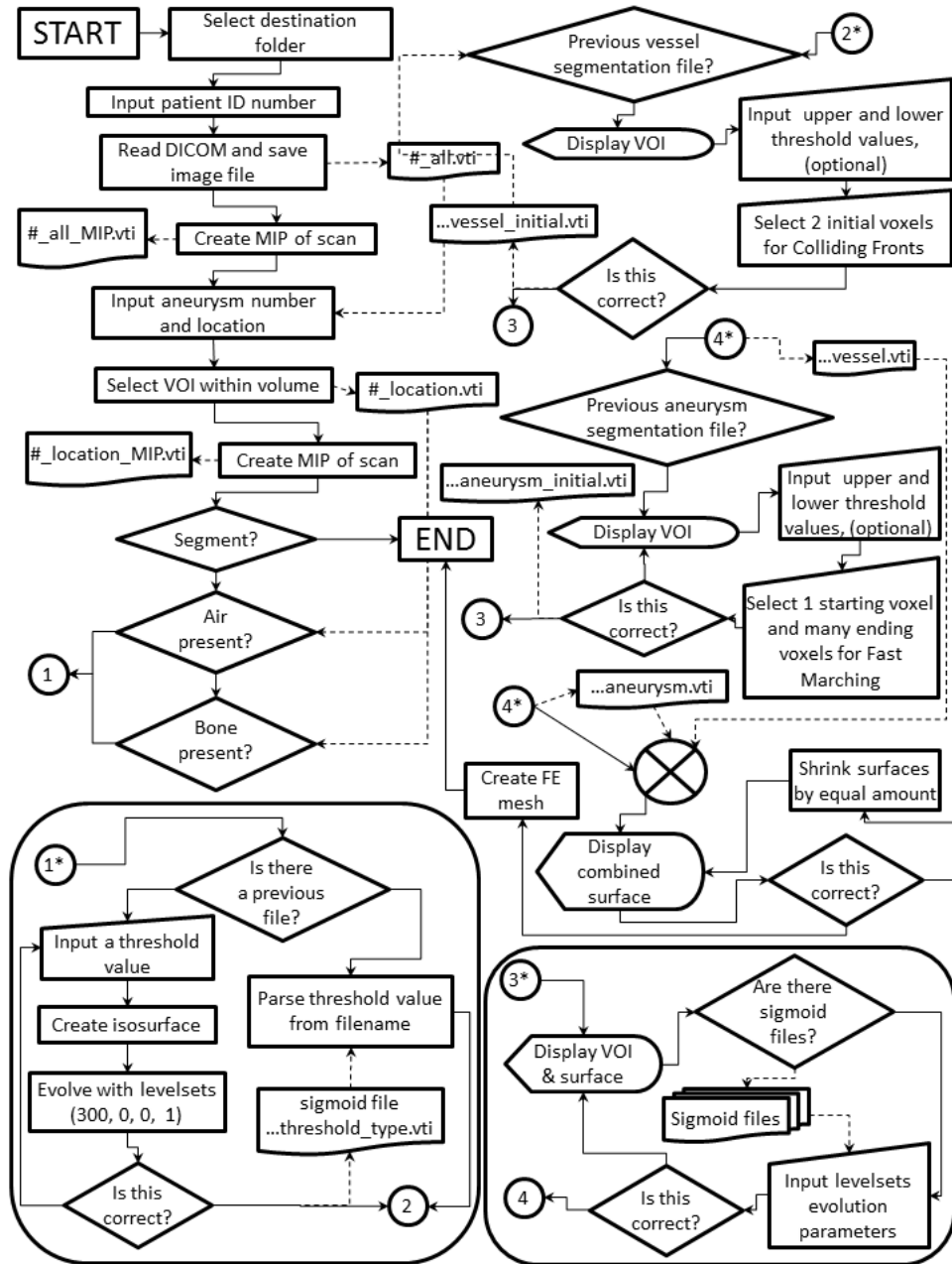
Figure B.7: Application flowchart

B.3 Protocol Code

```bash
#!/bin/bash
################################################################################
# Script:    aneurysm_bash_script.sh                                          #
# Task:      Moves user through a VMTK segmentation session with              #
#       explicit branch processes                                             #
# Requirements: Eye of Gnome image viewer                                     #
#       image file ".C_o_W.png"                                               #
#       VMTK                                                                   #
################################################################################
################################################################################
#                           global variables                                  #
################################################################################

SCRIPTNAME=$(basename ${0} .sh)
# Zenity variables
TITLE="BioMOST VMTK"
WIDTH=325
# Number of parameters needed (Edit line 55 logic)
NUMOFPARAMS=0
# Code testing parameters
DEBUGFILENAMES=1 # Zero=ON
DEBUGCOUNT=0
# exit status definitions
EXIT_SUCCESS=0
EXIT_FAILURE=1
EXIT_ERROR=2
EXIT_BUG=10
# variables for option switches with default values
VERBOSE="n"
OPTFOLDER=""
# variables for aneurysm segmentation
NOW=""
FILENAME=""
LOGIC=""
INITIAL=""
PICPATH="/var/tmp/dmwelch/uiowa/bash"
PICFILE=".CoW.png"
PATIENTPATH=""
PATIENT_NUM=""
DICOMPATH=""
```

```
TYPE=""
LEVEL=""
MESSAGE=""
AIRLEVEL=""
BONELEVEL=""
LEVELTYPE=""
ANEURYSM_NUM=1
ANEURYSM=1 #Equals false unless needed
###############################################################################
#                                functions                                    #
###############################################################################
function usage {
    echo "Usage: ${SCRIPTNAME} [-h] [-v] [-i] [-o folder]" >&2
    [[ ${#} -eq 1 ]] && exit ${1} || exit ${EXIT_FAILURE}
}

function debug {
    if [[ $DEBUGFILENAMES -eq 0 ]]
    then
        echo "${DEBUGCOUNT} -> $1"
        DEBUGCOUNT=$(( ${DEBUGCOUNT} + 1 ))
    fi
}

function interest_volume {
    zenity --question --width=$WIDTH --title=${TITLE} --text="Create a
    VOI?" --ok-label="_Yes" --cancel-label="_No"
    case $? in
        0)
            . get_location.sh  ;;
        1)
            FILENAME=`zenity --width=$WIDTH --title=${TITLE}
            --filename=${PATIENTPATH}/ --file-selection --title="Select
            VOI to use"`
            FILENAME=`basename ${FILENAME%%'.vti'}`
            vmtkimagereader -ifile ${PATIENTPATH}/${FILENAME}.vti --pipe
            vmtkimageviewer
            if [[ $DEBUGFILENAMES -eq 0 ]] ; then
                echo "${DEBUGCOUNT} -> ${FILENAME}"
                DEBUGCOUNT=$(( ${DEBUGCOUNT} + 1 ))
            fi ;;
        -1)
            exit ${EXIT_FAILURE} ;;
    esac
}
```

```
function create_sigmoid {
    zenity --width=$WIDTH --title="${TITLE}" --question --text="Does this
    VOI need $1 corrections?" --ok-label="_Yes" --cancel-label="_No"
    case $? in
        0)
            create_feature ;;
    -1 | 1)
            ;;
        *)
            echo $? ; exit ${EXIT_BUG}
    esac
}

function air_feature {
    LEVEL=`zenity --entry --title="${TITLE}" --width=$WIDTH --text="Enter
    the value for air" --cancel-label="_Done"`
    while [[ $? -eq 0 ]]
    do
        AIRLEVEL=$LEVEL
        vmtkimagereader -ifile ${PATIENTPATH}/${FILENAME}.vti --pipe
        vmtkmarchingcubes -l ${AIRLEVEL} --pipe vmtkrenderer --pipe
        vmtkimageviewer --pipe vmtksurfaceviewer
        LEVEL=`zenity --entry --title="${TITLE}" --width=$WIDTH --
        text="Enter the value for air" --cancel-label="_Done"`
    done
    LEVEL=$AIRLEVEL #Needed b/c last zenity call in while loop erases
    value for LEVEL!
}

function bone_feature {
    LEVEL=`zenity --entry --title="${TITLE}" --width=$WIDTH --text="Enter
    the value for bone" --cancel-label="_Done"`
    while [[ $? -eq 0 ]]
    do
        BONELEVEL=$LEVEL
        vmtkimagereader -ifile ${PATIENTPATH}/${FILENAME}.vti --pipe
        vmtkmarchingcubes -ifile ${PATIENTPATH}/${FILENAME}.vti -l
        ${BONELEVEL} --pipe vmtkrenderer --pipe vmtkimageviewer --pipe
        vmtksurfaceviewer
        LEVEL=`zenity --entry --title="${TITLE}" --width=$WIDTH --
        text="Enter the value for bone" --cancel-label="_Done"`
    done
    LEVEL=$BONELEVEL #Needed b/c last zenity call in while loop erases
    value for LEVEL!
```

```
    }

    function create_feature {
        zenity --question --width=$WIDTH --title=${TITLE} --text="Is there
        already a(n) ${TYPE} file?" --ok-label="_Yes" --cancel-label="_No"
        case $? in
            0) # Already a file
                LEVEL=`zenity --file-selection --title="${TITLE}: Select
                ${TYPE} file" --filename="${PATIENTPATH}/"`
                case $? in
                    0)
                        ;;
                    1)
                        echo "No file selected."
                        . quit.sh ;;
                    -1)
                        echo 'Zenity has caused an error!' # Something
                        happened with zenity
                        exit ${EXIT_ERROR} ;;
                    *)
                        echo $? ; exit ${EXIT_BUG}
                esac
                # Removes front and back from filename, leaving only LEVEL
                value
                LEVEL=${LEVEL%%.vti}
                LEVEL=${LEVEL##*${FILENAME}_${TYPE}_}
                # Now we need to pass the level value to the correct container
                variable
                if [[ ${TYPE} == 'air' ]]
                then
                    AIRLEVEL=${LEVEL}
                elif [[ ${TYPE} == 'bone' ]]
                then
                    BONELEVEL=${LEVEL}
                else
                    echo "Error assigning level values"; exit ${EXIT_BUG}
                fi
                ;;
            1) # No file
                ${TYPE}_feature
                if [[ ! -f
                ${PATIENTPATH}/${FILENAME}_${TYPE}_${LEVEL}_lvlset.vti ]]
                then
                    vmtklevelsetsegmentation -ifile
                    ${PATIENTPATH}/${FILENAME}.vti -ofeatureimagefile
```

```
                ${PATIENTPATH}/${FILENAME}_${TYPE}_${LEVEL}.vti -ofile
                ${PATIENTPATH}/${FILENAME}_${TYPE}_${LEVEL}_lvlset.vti
                vmtkimagefeaturecorrection -ifile
                ${PATIENTPATH}/${FILENAME}_${TYPE}_${LEVEL}.vti -
                levelsetsfile
                ${PATIENTPATH}/${FILENAME}_${TYPE}_${LEVEL}_lvlset.vti -
                scalefrominput 0 -ofile
                ${PATIENTPATH}/${FILENAME}_${TYPE}_sigmoid.vti
            fi ;;
    esac
}

function image_feature {
    vmtkimagecompose -ifile
    ${PATIENTPATH}/${FILENAME}_bone_${BONELEVEL}_lvlset.vti -i2file
    ${PATIENTPATH}/${FILENAME}_air_${AIRLEVEL}_lvlset.vti -negatei2 1 -
    ofile ${PATIENTPATH}/${FILENAME}_both_lvlset.vti
    vmtkimagefeaturecorrection -ifile
    ${PATIENTPATH}/${FILENAME}_bone_${BONELEVEL}.vti -levelsetsfile
    ${PATIENTPATH}/${FILENAME}_both_lvlset.vti -scalefrominput 0 -ofile
    ${PATIENTPATH}/${FILENAME}_both_sigmoid.vti
}

function segment {
    if [[ -f ${PATIENTPATH}/${NEWFILENAME}_initial.vti ]]
    then # IS
    initial file
        if [[ ! -f ${PATIENTPATH}/${FILENAME}_bone_sigmoid.vti && ! -f
        ${PATIENTPATH}/${FILENAME}_air_sigmoid.vti ]]
        then # NO sigmoid
        file
            vmtklevelsetsegmentation -ifile
            ${PATIENTPATH}/${FILENAME}.vti -initiallevelsetsfile
            ${PATIENTPATH}/${NEWFILENAME}_initial.vti -ofile
            ${PATIENTPATH}/${NEWFILENAME}_segm.vti
        else # IS initial & has sigmoid(s)
            if [[ -f ${PATIENTPATH}/${FILENAME}_bone_sigmoid.vti && -f
            ${PATIENTPATH}/${FILENAME}_air_sigmoid.vti ]]
            then
                if [[ ! $AIRLEVEL == "" && ! $BONELEVEL == "" ]]
                then
                    image_feature
                    echo "Both air and bone corrections detected"
                    LEVELTYPE="both"
                fi
```

```
            else
                if [[ -f ${PATIENTPATH}/${FILENAME}_bone_sigmoid.vti ]]
                then
                    echo "Only bone correction detected" ;
                    LEVELTYPE="bone"
                else
                    echo "Only air correction detected" ; LEVELTYPE="air"
                fi
            fi
            vmtklevelsetsegmentation -ifile ${PATIENTPATH}/${FILENAME}.vti
            -featureimagefile
            ${PATIENTPATH}/${FILENAME}_${LEVELTYPE}_sigmoid.vti -
            initiallevelsetsfile ${PATIENTPATH}/${NEWFILENAME}_initial.vti
            -ofile ${PATIENTPATH}/${NEWFILENAME}_segm.vti
        fi
    else # NO initial file
        if [[  ! -f ${PATIENTPATH}/${FILENAME}_bone_sigmoid.vti && ! -f
        ${PATIENTPATH}/${FILENAME}_air_sigmoid.vti ]]
        then # NO sigmoid file
            vmtkimageinitialization -ifile ${PATIENTPATH}/${FILENAME}.vti
            -olevelsetsfile ${PATIENTPATH}/${NEWFILENAME}_initial.vti
            vmtklevelsetsegmentation -ifile
            ${PATIENTPATH}/${FILENAME}.vti -initiallevelsetsfile
            ${PATIENTPATH}/${NEWFILENAME}_initial.vti -ofile
            ${PATIENTPATH}/${NEWFILENAME}_segm.vti
        else # NO initial & has sigmoid(s)
            if [[ -f ${PATIENTPATH}/${FILENAME}_bone_sigmoid.vti && -f
            ${PATIENTPATH}/${FILENAME}_air_sigmoid.vti ]]
            then
                image_feature
                echo "Both air and bone corrections detected" ;
                LEVELTYPE="both"
            else
                if [[ -f ${PATIENTPATH}/${FILENAME}_bone_sigmoid.vti ]]
                then
                    echo "Only bone correction detected" ;
                    LEVELTYPE="bone"
                else
                    echo "Only air correction detected" ; LEVELTYPE="air"
                fi
            fi
            vmtkimageinitialization -ifile ${PATIENTPATH}/${FILENAME}.vti
            -olevelsetsfile ${PATIENTPATH}/${NEWFILENAME}_initial.vti
            vmtklevelsetsegmentation -ifile ${PATIENTPATH}/${FILENAME}.vti
            -initiallevelsetsfile
```

```
                    ${PATIENTPATH}/${NEWFILENAME}_initial.vti -featureimagefile
                    ${PATIENTPATH}/${FILENAME}_${LEVELTYPE}_sigmoid.vti -ofile
                    ${PATIENTPATH}/${NEWFILENAME}_segm.vti
            fi
    fi
    REPLY=""
    echo "Please record the evolution smoothing parameters"
    echo "you used and the vessels they were applied to:"
    echo "Type \"q\" or \"Q\" to quit"
    while [[ ! $REPLY == "q" && ! $REPLY == "Q" ]]
    do
        read
        if  [[ ! $REPLY == "q" && ! $REPLY == "Q" ]]; then
            echo $REPLY 1>>$PATIENTPATH/levelsetparams${ANEURYSM_NUM}
        fi
    done
}


function combine {
    VESSEL=`zenity --file-selection --filename=$PATIENTPATH/
    --title="${TITLE}: Select vessel file"`; VESSEL=${VESSEL%%'.vti'}
    ANEURYSM=`zenity --file-selection --filename=$PATIENTPATH/
    --title="${TITLE}: Select aneurysm file"`
    ANEURYSM=${ANEURYSM%%'.vti'}
    vmtkimagecompose -ifile ${VESSEL}.vti -i2file ${ANEURYSM}.vti
    -operation min -ofile ${PATIENTPATH}/${FILENAME}_combined_segm.vti
    --pipe vmtkmarchingcubes -i @vmtkimagecompose.o --pipe
    vmtksurfaceviewer
    vmtkimagereslice -spacing 0.25 0.25 0.25 -ifile ${VESSEL}.vti -ofile
    ${VESSEL}_sub.vti
    vmtkimagereslice -spacing 0.25 0.25 0.25 -ifile ${ANEURYSM}.vti -ofile
    ${ANEURYSM}_sub.vti
    YESNO=1
    while [[ ! $YESNO == 0 ]]
    do
        SHIFT=`zenity --entry --title="${TITLE}" --width=$WIDTH
        --text="Enter the magnitude to shrink (0-1)"`
        vmtkimageshiftscale -ifile ${VESSEL}_sub.vti -shift $SHIFT -ofile
        ${VESSEL}_sub_shrinked.vti
        vmtkimageshiftscale -ifile ${ANEURYSM}_sub.vti -shift $SHIFT
        -ofile ${ANEURYSM}_sub_shrinked.vti
        vmtkimagecompose -ifile ${VESSEL}_sub_shrinked.vti -i2file
        ${ANEURYSM}_sub_shrinked.vti -operation min -ofile
        ${PATIENTPATH}/${FILENAME}_combined_segm.vti  --pipe
        vmtkmarchingcubes -i @vmtkimagecompose.o --pipe vmtksurfaceviewer
```

```
        'zenity --question --title="$TITLE" --text="Is this satisfactory?"
        --ok-label="_Yes" --cancel-label="_No"'
        YESNO=$?
    done
    echo "Shift scale value is ${SHIFT} for ${FILENAME}_segm.vtp\n $DATE"
    1<${PATIENTPATH}/shiftscale.txt
}
###############################################################################
#                              main program                                   #
###############################################################################
# the options -h for help should always be present. Options -v and
# -o are examples. -o needs a parameter, indicated by the colon ":"
# following in the getopts call
while getopts ':o:vh' OPTION ; do
    case ${OPTION} in
        v)  VERBOSE=y ;;
        o)  OPTFOLDER="${OPTARG}" ;;
        i)  INITIAL=y ;; #This is the first segmentation and the dicom
            folder needs read
        h)  usage ${EXIT_SUCCESS} ;;
       \?)  echo "unknown option \"-${OPTARG}\"." >&2
            usage ${EXIT_ERROR} ;;
        :)  echo "option \"-${OPTARG}\" requires an argument." >&2
            usage ${EXIT_ERROR} ;;
        *)  echo "Impossible error. parameter: ${OPTION}" >&2
            usage ${EXIT_BUG} ;;
    esac
done
shift $(( OPTIND - 1 )) # skip parsed options
if [[ $# -lt $NUMOFPARAMS ]]
then
    echo 'Wrong number of parameters' >&2
    usage ${EXIT_ERROR} ; exit
fi
for ARG # loop through all arguments
do
    if [[ ${VERBOSE} = y ]]
    then
        echo -n 'argument: '
    fi
    echo ${ARG}
done
# Needed on BIOMOST000
# export PYTHONPATH=/usr/css/opt/vmtk-0.8/lib:
# /usr/css/opt/vmtk-0.8/lib/vmtk:
```

```
# /usr/css/opt/vtk-5.4.2/lib64/python2.6/site-packages
# export LD_LIBRARY_PATH=/usr/css/opt/vtk-5.4.2/lib/vtk-5.4:
# /usr/css/opt/InsightToolkit-3.16.0/lib/InsightToolkit:
# /usr/css/opt/vmtk-0.8/lib:/usr/css/opt/vmtk-0.8/lib/vmtk
NOW=`date`
xhost +local:$USER
. get_patient_path.sh; FILENAME=$PATIENT_NUM; debug FILENAME
. aneurysm_num.sh;      FILENAME=$FILENAME;    debug FILENAME
. get_dicom_path.sh
COUNT=1
while [[ $COUNT -le $ANEURYSM_NUM ]]
do
# Loop following code or ask to select which to do
    FILENAME="${PATIENT_NUM}_${COUNT}";        debug FILENAME
    interest_volume
    zenity --width=$WIDTH --title="${TITLE}" --question --text="Would you
    like to segment this VOI?" --ok-label="_Yes" --cancel-label="_No"
    case $? in
        0)
            TYPE="air"; create_sigmoid $TYPE;
            TYPE="bone"; create_sigmoid $TYPE;
            for NEWFILENAME in "$FILENAME" "${FILENAME}_aneurysm"
            do
                if [[ -f ${PATIENTPATH}/${NEWFILENAME}_segm.vti ]]
                then
                    # This has a previous completed segmentation
                    zenity --width=$WIDTH --title="${TITLE}" --question
                    --text="Would you like to use the existing segmented
                    model\n for $NEWFILENAME?" --ok-label="_Yes"
                    --cancel-label="_No"
                    case $? in
                        0)
                            vmtkimagereader -ifile
                            ${PATIENTPATH}/${NEWFILENAME}_segm.vti --pipe
                            vmtkmarchingcubes -l 0.0 --pipe vmtkrenderer
                            --pipe vmtkimagereader -ifile
                            ${PATIENTPATH}/${FILENAME}.vti --pipe
                            vmtkimageviewer --pipe vmtksurfaceviewer
                            # Show model to user and proceed
                            ;;
                        1)
                            segment # If there is a previous model but we
                            want to make a new one...
                            ;;
                    esac
```

```
                else
                    segment # If there is no previous model, make one...
                fi
            done
        combine ;;
    -1 | 1)
        exit ${EXIT_SUCCESS} ;; # No, do nothing and exit
    esac
    . reconstruct.sh
    if [[ ${FILENAME} == *CoW* ]]
    then
        echo "Renaming CoW folders"
        for ii in `find . -name "CoW" -type f`
        do
            mv $ii "${ii%"_${COUNT}_"*}_${ii##*"_${COUNT}_"}"
        done
        COUNT=${COUNT}; # Don't advance the count for CoW
    else
        COUNT=${COUNT}+1;
    fi
    FILENAME=$PATIENT_NUM # Reset the filename
done
exit ${EXIT_SUCCESS}
#!/bin/bash
################################################################################
# Script:   reconstruct.sh                                                     #
# Task:         This script searches for files ending in _segm.vti and         #
#       passes the batch of them through a meshing and centerline  #
#       analysis.  Other methods will be implemented in future      #
#                 This can be run as a stand-alone program.                    #
# Author:     Dave Welch                                                       #
# Contact:    david.m.welch@gmail.com                                          #
# Date:       10 Feb, 2010                                                     #
# Licence:    Copyright (C) 2010 David M. Welch                                #
#                                                                              #
# This program is free software: you can redistribute it and/or modify    #
#    it under the terms of the GNU General Public License as published by  #
#    the Free Software Foundation, either version 3 of the License, or     #
#    (at your option) any later version.                                   #
#                                                                              #
#    This program is distributed in the hope that it will be useful,       #
#    but WITHOUT ANY WARRANTY; without even the implied warranty of        #
#    MERCHANTABILITY or FITNESS FOR A PARTICULAR PURPOSE.  See the         #
#    GNU General Public License for more details.                          #
#    You should have received a copy of the GNU General Public License     #
```

```
#    along with this program.  If not, see <http://www.gnu.org/licenses/>. #
#                                                                          #
############################################################################
############################################################################
#                          global variables                               #
############################################################################
SCRIPTNAME=$(basename ${0} .sh)

# Number of parameters needed (Edit line 55 logic)
NUMOFPARAMS=0

EXIT_SUCCESS=0
EXIT_FAILURE=1
EXIT_ERROR=2
EXIT_BUG=10

# variables for option switches with default values
VERBOSE="n"
OPTFILE=""
LICENSE="COPYING"

############################################################################
#                              functions
############################################################################
function usage {
    echo "Usage: ${SCRIPTNAME} [-h] [-v] [-c] [-o arg] file ..." >&2
    [[ ${#} -eq 1 ]] && exit ${1} || exit ${EXIT_FAILURE}
}

function copyright {
        DIR=`find / -type d -name "name" 2>/dev/null`
        exec < "${DIR}/${LICENSE}"
        while read LINE ; do
                echo ${LINE}
        done
}

############################################################################
#                              main program
############################################################################

# the options -h for help should always be present. Options -v and
# -o are examples. -o needs a parameter, indicated by the colon ":"
# following in the getopts call
while getopts ':o:vhc' OPTION ; do
```

```
        case ${OPTION} in
                c)      copyright
                        ;;
            v)  VERBOSE=y
                ;;
            o)  OPTFILE="${OPTARG}"
                ;;
            h)  usage ${EXIT_SUCCESS}
                ;;
            \?) echo "unknown option \"-${OPTARG}\"." >&2
                usage ${EXIT_ERROR}
                ;;
            :)  echo "option \"-${OPTARG}\" requires an argument." >&2
                usage ${EXIT_ERROR}
                ;;
            *)  echo "Impossible error. parameter: ${OPTION}" >&2
                usage ${EXIT_BUG}
                ;;
        esac
done

# skip parsed options
shift $(( OPTIND - 1 ))

# if you want to check for a minimum or maximum number of arguments,
# do it here
if [[ $# -ne $NUMOFPARAMS ]] ; then
    echo "Wrong number of parameters" >&2
    usage ${EXIT_ERROR}
fi

# loop through all arguments
for ARG ; do
    if [[ ${VERBOSE} = y ]] ; then
        echo -n "argument: "
    fi
    echo ${ARG}
done
if [[ -z ${PATIENTPATH} ]] ; then
        . get_patient_path.sh
        # Needed on BIOMOST000
        #export PYTHONPATH=/usr/css/opt/vmtk-0.8/lib:...
            /usr/css/opt/vmtk-0.8/lib/vmtk:/usr/css/opt/...
            vtk-5.4.2/lib64/python2.6/site-packages
        #export LD_LIBRARY_PATH=/usr/css/opt/vtk-5.4.2/lib...
```

```
            /vtk-5.4:/usr/css/opt/InsightToolkit-3.16.0/...
            lib/InsightToolkit:/usr/css/opt/vmtk-0.8/lib:...
            /usr/css/opt/vmtk-0.8/lib/vmtk
fi

INPUT=`zenity --file-selection --filename=$PATIENTPATH/...
    --title="Select segm file to mesh"`

vmtkmarchingcubes -ifile ${INPUT} --pipe vmtksurfacetriangle ...
-pipe vmtksurfacewriter -f tecplot -ofile ${INPUT%%.vti}.dat
# Tecplot files need .dat extention, but no interior manipulations

tecplot ${INPUT%%segm.vti}mesh.dat
exit ${EXIT_SUCCESS}
```

REFERENCES

[1] Luca Antiga. *Patient-Specific Modeling of Geometry and Blood Flow in Large Arteries.* PhD thesis, Politecnico Di Milano, 2002.

[2] Luca Antiga, Marina Piccinelli, Lorenzo Botti, Bogdan Ene-Iordache, Andrea Remuzzi, and David A. Steinman. An image-based modeling framework for patient-specific computational hemodynamics. *Med Biol Eng Comput*, 46(11):1097–112, 2008.

[3] Y. Asai, Y. Shintani, M. Yamaguchi, M. Uemura, M. Matsumoto, and H. Kanamori. Evaluation of grey-scale standard display function as a calibration tool for diagnostic liquid crystal display monitors using psychophysical analysis. *Medical and Biological Engineering and Computing*, 43(3):319–324, 2005.

[4] S. W. Atlas. MR angiography in neurologic disease. *Radiology*, 193(1):1–16, 1994.

[5] Klaus Bacher. *Evaluation of image quality and patient radiation dose in digital radiology.* PhD thesis, Universiteit Gent, May 2006.

[6] M. Banatwala, C. Farley, D. Feinberg, and J. D. Humphrey. Parameterization of the shape of intracranial saccular aneurysms using legendre polynomials. *Comput Methods Biomech Biomed Engin*, 8(2):93–101, 2005.

[7] Juan R. Cebral, Marcelo A. Castro, James E. Burgess, Richard S. Pergolizzi, Michael J. Sheridan, and Christopher M. Putman. Characterization of cerebral aneurysms for assessing risk of rupture by using patient-specific computational hemodynamics models. *Am J Neuroradiol*, 26(10):2550–2559, 2005.

[8] Juan R. Cebral, Monica Hernandez, Alejandro Frangi, Christopher Putman, Richard Pergolizzi, and James Burgess. Subject-specific modeling of intracranial aneurysms. *Medical Imaging 2004: Physiology, Function, and Structure from Medical Images*, 5369(1):319–327, 2004.

[9] Juan Raul Cebral and Rainald Löhner. From medical images to anatomically accurate finite element grids. *International Journal for Numerical Methods in Engineering*, 51(8):985–1008, 2001.

[10] Cybèle Ciofolo and Christian Barillot. Atlas-based segmentation of 3d cerebral

structures with competitive level sets and fuzzy control. *Med Image Anal*, 13(3):456–70, 2009.

[11] M. R. Crompton. Mechanism of growth and rupture in cerebral berry aneurysms. *British Medical Journal*, 1(5496):1138–42, 1966, May 7.

[12] S. M. de la Monte, G. W. Moore, M. A. Monk, and G. M. Hutchins. Risk factors for the development and rupture of intracranial berry aneurysms. *Am. J. Med.*, 78(6 Pt 1):957–64, 1985.

[13] Nicolien de Rooij, Birgitta Velthuis, Ale Algra, and Gabriël Rinkel. Configuration of the circle of willis, direction of flow, and shape of the aneurysm as risk factors for rupture of intracranial aneurysms. *Journal of Neurology*, 256(1):45–50, 2009.

[14] S. Dhar, M. Tremmel, J. Mocco, M. Kim, J. Yamamoto, A. H. Siddiqui, L. N. Hopkins, and H. Meng. Morphology parameters for intracranial aneurysm rupture risk assessment. *Neurosurgery*, 63:185–196, Aug 2008.

[15] R. R. Edelman. Mr angiography: present and future. *AJR Am J Roentgenol*, 161:1–11, Jul 1993.

[16] D. F. Elger, D. M. Blackketter, R. S. Budwig, and K. H. Johansen. The influence of shape on the stresses in model abdominal aortic aneurysms. *J Biomech Eng*, 118:326–332, Aug 1996.

[17] Azadeh Firouzian, Rashindra Manniesing, Zwenneke H. Flach, Roelof Risselada, Fop van Kooten, Miriam C. J. M. Sturkenboom, Aad van der Lugt, and Wiro J. Niessen. Intracranial aneurysm segmentation in 3d CT angiography: Method and quantitative validation with and without prior noise filtering. *European Journal of Radiology*, In Press, Corrected Proof, 2010.

[18] M. D. Ford, Y. Hoi, M. Piccinelli, L. Antiga, and D. A. Steinman. An objective approach to digital removal of saccular aneurysms: technique and applications. *Br J Radiol*, 82(Special Issue 1):S55–61, Jun 2009.

[19] T. R. Forget, R. Benitez, E. Veznedaroglu, A. Sharan, W. Mitchell, M. Silva, and R. H. Rosenwasser. A review of size and location of ruptured intracranial aneurysms. *Neurosurgery*, 49:1322–1325, Dec 2001.

[20] George N. Foutrakis, Howard Yonas, and Robert J. Sclabassi. Saccular aneurysm formation in curved and bifurcating arteries. *AJNR Am J Neuroradiol*, 20(7):1309–1317, 1999.

[21] T. Lui Grant, Nicholas J. Volpe, and Steven Galetta. *Neuro-ophthalmology : diagnosis and management.* Saunders Elsevier, Philadelphia, 2nd edition, 2010.

[22] Alain Herment, Nadjia Kachenoura, Muriel Lefort, Mourad Bensalah, Anas Dogui, Frédérique Frouin, Elie Mousseaux, and Alain De Cesare. Automated segmentation of the aorta from phase contrast MR images: Validation against expert tracing in healthy volunteers and in patients with a dilated aorta. *Journal of Magnetic Resonance Imaging*, 31(4):881–888, 2010.

[23] Monica Hernandez, Alejandro F. Frangi, and Guillermo Sapiro. Three-dimensional segmentation of brain aneurysms in cta using non-parametric region-based information and implicit deformable models: Method and evaluation. In *Medical Image Computing and Computer-Assisted Intervention - MICCAI 2003*. Springer Berlin / Heidelberg, 2003.

[24] B. L. Hoh, C. L. Sistrom, C. S. Firment, G. L. Fautheree, G. J. Velat, J. H. Whiting, J. F. Reavey-Cantwell, and S. B. Lewis. Bottleneck factor and height-width ratio: association with ruptured aneurysms in patients with multiple cerebral aneurysms. *Neurosurgery*, 61:716–722, Oct 2007.

[25] L. Ibanez, W. Schroeder, L. Ng, and J. Cates. *The ITK Software Guide.* http://www.itk.org/ItkSoftwareGuide.pdf, second edition, 2005.

[26] Tetsuji Inagawa and Asao Hirano. Autopsy study of unruptured incidental intracranial aneurysms. *Surgical Neurology*, 34(6):361, 1990.

[27] Tetsuji Inagawa and Asao Hirano. Ruptured intracranial aneurysms: An autopsy study of 133 patients. *Surgical Neurology*, 33(2):117, 1990.

[28] Haruo Isoda, Yasuo Takehara, Satoshi Isogai, Hatsuko Masunaga, Hiroyasu Takeda, Atsushi Nozaki, and Harumi Sakahara. MRA of intracranial aneurysm models: A comparison of contrast-enhanced three-dimensional MRA with Time-of-Flight MRA. *Journal of Computer Assisted Tomography*, 24(2), 2000.

[29] S. Claiborne Johnston, Charles B. Wilson, Van V. Halbach, Randall T. Higashida, Christopher F. Dowd, Michael W. McDermott, Carol B. Applebury, Thomas L. Farley, and Daryl R. Gress. Endovascular and surgical treatment of unruptured cerebral aneurysms: Comparison of risks. *Annals of Neurology*, 48(1):11–19, 2000.

[30] S. K. Kyriacou and J. D. Humphrey. Influence of size, shape and properties on the mechanics of axisymmetric saccular aneurysms. *J Biomech*, 29:1015–1022,

Aug 1996.

[31] Ming-Hua Li, Ying-Sheng Cheng, Yong-Dong Li, Chun Fang, Shi-Wen Chen, Wu Wang, Ding-Jun Hu, and Hao-Wen Xu. Large-cohort comparison between three-dimensional time-of-flight magnetic resonance and rotational digital subtraction angiographies in intracranial aneurysm detection. *Stroke*, 40(9):3127–9, 2009.

[32] William E. Lorensen and Harvey E. Cline. Marching cubes: A high resolution 3D surface construction algorithm. *SIGGRAPH Comput. Graph.*, 21(4):163–169, Aug 1987.

[33] Baoshun Ma, Robert E. Harbaugh, and Madhavan Raghavan. Three-dimensional geometrical characterization of cerebral aneurysms. *Annals of Biomedical Engineering*, 32(2):264–273, 2004.

[34] R. Malladi, J. A. Sethian, and B. C. Vemuri. Topology-independent shape modeling scheme. In B. C. Vemuri, editor, *Society of Photo-Optical Instrumentation Engineers (SPIE) Conference Series*, volume 2031 of *Society of Photo-Optical Instrumentation Engineers (SPIE) Conference Series*, pages 246–258, Jun 1993.

[35] R. Manniesing, M. A. Viergever, and W. J. Niessen. Vessel enhancing diffusion - a scale space representation of vessel structures. *Medical Image Analysis*, 10(6):815–825, 2006.

[36] M. J. McAuliffe, F. M. Lalonde, D. McGarry, W. Gandler, K. Csaky, and B. L. Trus. Medical image processing, analysis & visualization in clinical research. *IEEE Computer-based Medical Systems (CBMS)*, pages 381–386, 2001.

[37] Charles A. McDonald and Milton Korb. Intracranial aneurysms. *Arch Neurol Psychiatry*, 42(2):298–328, 1939.

[38] J P Mesirov. Accessible reproducible research. *Science*, 327(5964):415–416, 2010.

[39] R. D. Millan, L. Dempere-Marco, J. M. Pozo, J. R. Cebral, and A. F. Frangi. Morphological characterization of intracranial aneurysms using 3-D moment invariants. *Medical Imaging, IEEE Transactions on*, 26(9):1270–1282, Sept 2007.

[40] Raul D. Millan, Monica Hernandez, Daniel Gallardo, Juan R. Cebral, Christopher Putman, Laura Dempere-Marco, and Alejandro F. Frangi. Characterization of cerebral aneurysms using 3d moment invariants. In *Proceedings of SPIE*.

[41] B. E. Muhs, P. Gagne, J. Wagener, J. Baker, M. R. Ortega, M. A. Adelman, N. S. Cayne, C. B. Rockman, and T. Maldonado. Gadolinium-enhanced versus time-of-flight magnetic resonance angiography: what is the benefit of contrast enhancement in evaluating carotid stenosis? *Ann Vasc Surg*, 19:823–828, Nov 2005.

[42] M. Okahara. Diagnostic accuracy of magnetic resonance angiography for cerebral aneurysms in correlation with 3D-digital subtraction angiographic images: A study of 133 aneurysms. *Stroke*, 33(7):1803, 2002.

[43] Luciana Parlea, Rebecca Fahrig, David W. Holdsworth, and Stephen P. Lownie. An analysis of the geometry of saccular intracranial aneurysms. *AJNR Am J Neuroradiol*, 20(6):1079–1089, 1999.

[44] M. Piccinelli, A. Veneziani, D. A. Steinman, A. Remuzzi, and L. Antiga. A framework for geometric analysis of vascular structures: Application to cerebral aneurysms. *Medical Imaging, IEEE Transactions on*, 28(8):1141–1155, Aug 2009.

[45] M. Piotin, P. Gailloud, L. Bidaut, S. Mandai, M. Muster, J. Moret, and D. A. Rüfenacht. Ct angiography, mr angiography and rotational digital subtraction angiography for volumetric assessment of intracranial aneurysms. an experimental study. *Neuroradiology*, 45(6):404–9, 2003.

[46] Madhavan Raghavan, Baoshun Ma, and Robert E. Harbaugh. Quantified aneurysm shape and rupture risk. *Journal of Neurosurgery*, 102(Feb):355, 2005.

[47] Maryam Rahman, Janel Smietana, Erik Hauck, Brian Hoh, Nick Hopkins, Adnan Siddiqui, Elad I. Levy, Hui Meng, and J. Mocco. Size ratio correlates with intracranial aneurysm rupture status: A prospective study. *Stroke*, 41(5):916–920, 2010.

[48] L. A. Rogers. Intracranial aneurysm size and potential for rupture. *J. Neurosurg.*, 67(3):475–6, 1987.

[49] W. I. Schievink, D. G. Piepgras, and F. P. Wirth. Rupture of previously documented small asymptomatic saccular intracranial aneurysms. report of three cases. *J. Neurosurg.*, 76(6):1019–24, 1992.

[50] Will Schroeder, Ken Martin, and Bill Lorensen. *The Visualization Toolkit: An Object-Oriented Approach to 3D Graphics*. Kitware, Inc., Columbia, 4th edition, 2006.

[51] M. Schwab, N. Karrenbach, and J. Claerbout. Making scientific computations reproducible. *Computing in Science Engineering*, 2(6):61–67, Nov/Dec 2000.

[52] P. Seshaiyer, F. P. K. Hsu, A. D. Shah, S. K. Kyriacou, and J. D. Humphrey. Multiaxial mechanical behavior of human saccular aneurysms. *Computer Methods in Biomechanics and Biomedical Engineering*, 4(3):281, 2001.

[53] J. A. Sethian. *Level Set Methods and Fast Marching Methods*. Cambridge University Press, New York, NY, 2nd edition, 1999.

[54] Pankaj K. Singh, Alberto Marzo, Bethany Howard, Daniel A. Rufenacht, Philippe Bijlenga, Alejandro F. Frangi, Patricia V. Lawford, Stuart C. Coley, D. Rodney Hose, and Umang J. Patel. Effects of smoking and hypertension on wall shear stress and oscillatory shear index at the site of intracranial aneurysm formation. *Clinical Neurology and Neurosurgery*, In Press, Corrected Proof, 2010.

[55] H. Ujiie, K. Sato, H. Onda, A. Oikawa, M. Kagawa, K. Takakura, and N. Kobayashi. Clinical analysis of incidentally discovered unruptured aneurysms. *Stroke*, 24:1850–1856, Dec 1993.

[56] H. Ujiie, H. Tachibana, O. Hiramatsu, A. L. Hazel, T. Matsumoto, Y. Ogasawara, H. Nakajima, T. Hori, K. Takakura, and F. Kajiya. Effects of size and shape (aspect ratio) on the hemodynamics of saccular aneurysms: a possible index for surgical treatment of intracranial aneurysms. *Neurosurgery*, 45(1):119–29; discussion 129–30, 1999.

[57] Ritva Vanninen, Timo Koivisto, Tapani Saari, Juha Hernesniemi, and Matti Vapalahti. Ruptured intracranial aneurysms: Acute endovascular treatment with electrolytically detachable coils—a prospective randomized study. *Radiology*, 211(2):325–336, 1999.

[58] Michael S. Vaphiades and Joseph A. Horton. MRA or CTA, that's the question. *Surv Ophthalmol*, 50(4):406–10, 2005.

[59] Bryce Weir. Unruptured intracranial aneurysms: a review. *J. Neurosurg.*, 96(1):3–42, 2002.

[60] Philip M. White, Evelyn M. Teasdale, Joanna M. Wardlaw, and Valerie Easton.

Intracranial aneurysms: CT angiography and MR angiography for detection—prospective blinded comparison in a large patient cohort. *Radiology*, 219(3):739–749, 2001.

[61] Philip M. White, Joanna M. Wardlaw, and Valerie Easton. Can noninvasive imaging accurately depict intracranial aneurysms?: A systematic review. *Radiology*, 217(2):361–370, 2000.

[62] T Yoo and D Metaxas. Open science - combining open data and open source software: Medical image analysis with the insight toolkit. *Medical Image Analysis*, 9(6):503–506, Dec 2005.

[63] X. Zhao, Y. Yin, B. Yang, B. Zhu, and X. Tian. Level set and geodesic active contours based measurement of material removal between serial sections. *Computational Materials Science*, 39(4):857, 2007.

[64] Kelly H. Zou, Kemal Tuncali, Simon K. Warfield, Christian P. Zentai, Daniel Worku, Paul R. Morrison, and Stuart G. Silverman. Three-dimensional assessment of MR imaging-guided percutaneous cryotherapy using multi-performer repeated segmentations: the value of supervised learning. *Academic Radiology*, 12(4):444–50, 2005.